HHS Public Access

Author manuscript

J Mol Biol. Author manuscript; available in PMC 2017 March 27.

Published in final edited form as:

J Mol Biol. 2016 March 27; 428(6): 1107–1129. doi:10.1016/j.jmb.2015.02.008.

The PRE-Derived NMR Model of the 38.8 kDa Tri-Domain IsdH Protein from *Staphylococcus aureus* Suggests that it Adaptively Recognizes Human Hemoglobin

Megan Sjodt[a,b,c], **Ramsay Macdonald**[a,b,c], **Thomas Spirig**[a], **Albert H. Chan**[a,b,c], **Claire F. Dickson**[e], **Marian Fabian**[d], **John S. Olson**[d], **David A. Gell**[e], and **Robert T. Clubb**[a,b,c,*]

[a]Department of Chemistry and Biochemistry, University of California, Los Angeles, 611 Charles Young Drive East, Los Angeles, CA 90095, USA

[b]UCLA-DOE Institute of Genomics and Proteomics, University of California, Los Angeles, 611 Charles Young Drive East, Los Angeles, CA 90095, USA

[c]Molecular Biology Institute, University of California, Los Angeles, 611 Charles Young Drive East, Los Angeles, CA 90095, USA

[d]Department of Biochemistry and Cell Biology, Rice University, Houston, Texas 77251

[e]Menzies Research Institute Tasmania, University of Tasmania, Hobart, Tasmania 7000, Australia

Abstract

Staphylococcus aureus is a medically important bacterial pathogen that during infections acquires iron from human hemoglobin (Hb). It uses two closely related iron regulated surface determinant (Isd) proteins to capture and extract the oxidized form of heme (hemin) from Hb, IsdH and IsdB. Both receptors rapidly extract hemin using a conserved tri-domain unit consisting of two NEAr iron Transporter (NEAT) domains connected by a helical linker domain. To gain insight into the mechanism of extraction we used NMR to investigate the structure and dynamics of the 38.8 kDa tri-domain IsdH protein (IsdH^{N2N3}, A326-D660 with a Y642A mutation that prevents hemin binding). The structure was modeled using long-range paramagnetic relaxation enhancement (PRE) distance restraints, dihedral angle, small angle x-ray scattering, residual dipolar coupling and inter-domain NOE data. The receptor adopts an extended conformation wherein the linker and N3 domains pack against each other via a hydrophobic interface. In contrast, the N2 domain contacts the linker domain via a hydrophilic interface, and based on NMR relaxation data undergoes inter-domain motions enabling it to reorient with respect to the body of the protein. Ensemble calculations were used to estimate the range of N2 domain positions compatible with the PRE data. A comparison of the Hb-free and -bound forms reveals that Hb binding alters the positioning of the N2 domain. We propose that binding occurs through a combination of conformational selection and induced fit mechanisms that may promote hemin release from Hb by altering the position of its F-helix.

*To whom correspondence should be addressed: Dept. of Chemistry and Biochemistry, University of California, Los Angeles, 602 Boyer Hall, Los Angeles, CA 90095. Tel.: 310-206-2334; Fax: 310-206-4749; rclubb@mbi.ucla.edu.

Keywords

Paramagnetic relaxation enhancement; Large protein NMR; Iron regulated surface determinant system; Hemoglobin receptor; Nuclear magnetic resonance spectroscopy

Introduction

Staphylococcus aureus causes a range of illnesses from minor skin infections, to life-threatening diseases such as meningitis, pneumonia, osteomyelitis, endocarditis, toxic shock syndrome and septicemia[1]. In the United States *S. aureus* is a leading cause of life-threatening hospital and community acquired infections[2]. There is a growing need to understand the mechanism through which it causes disease as many strains of *S. aureus* have become resistant to conventional antibiotics, such as highly virulent methicillin-resistant strains of *S. aureus* (MRSA). *S. aureus'* ability to replicate within its host is critically dependent on access to iron, since this metal functions as a key biocatalyst and/or electron carrier in microbial enzymes that mediate metabolism[3]. Free iron is scarce in the human body and must therefore be actively procured during infections[4]. Heme (Iron-protoporphyrin IX) bound to human hemoglobin (Hb) contains ~75–80% of the body's total iron content and is preferentially utilized by *S. aureus*[5]. An understanding of how *S. aureus* captures Hb and extracts its heme is therefore of fundamental importance and could potentiate the development of novel antimicrobial agents that work by disrupting heme acquisition.

S. aureus acquires heme-iron from human Hb using nine iron-regulated surface determinant (Isd) proteins[6–8]. Four Isd proteins (IsdA, IsdB, IsdC, and IsdH/HarA) bind heme and are covalently linked to the peptidoglycan cell wall by sortase transpeptidases[9–11]. Biochemical and cellular localization studies suggest that heme capture and transfer across the cell wall is mediated by an ordered set of heme transfer reactions. In this process, IsdB and IsdH first bind Hb and extract its heme[10,12]. Heme is then passed from IsdB/IsdH to IsdA, which is partially buried within the cell wall. Next, IsdA passes heme to the IsdC protein, which has recently been shown to occur via a transient ultra-weak IsdA-IsdC heme transfer complex[10,13–16]. Holo-IsdC then delivers the heme to the IsdDEF complex, a bacterial ABC transporter that pumps heme into the cytoplasm. Free iron is then obtained when the heme oxidase, IsdG (or its paralog IsdI), degrades heme [17,18]. Hb and heme binding by the IsdA, IsdB, IsdC, and IsdH proteins is mediated by NEAr iron Transporter (NEAT) domains. These conserved binding modules are ~125 residues in length and were originally named based on the location of their parent genes, which are typically proximal to genes encoding putative Fe^{3+} siderophore transporter genes[19]. NEAT domains adopt a conserved β-sandwich fold and depending upon the domain, can bind to distinct ligands, including heme, Hb, haptoglobin, and other host proteins[20–23]. Additionally, these domains are also found in other Gram-positive bacteria containing systems similar to the Isd system[19,24,25].

The IsdB and IsdH surface receptors each contain a highly conserved tri-domain unit that rapidly extracts heme from Hb[26]. In IsdH, the tri-domain unit consists of the second (N2) and third (N3) NEAT domains that are connected by a helical linker domain (Fig. 1a). The NEAT domains have distinct functions, N2 binds Hb, while the N3 domain binds to

heme[20,22,27]. Heme extraction by the tri-domain occurs up to ~270 times faster than the rate at which Hb spontaneously releases heme into the solvent[26,28] (Fig. 1b–d). All three domains are required for rapid heme extraction from Hb and must be located within the same polypeptide chain to function synergistically. IsdB likely operates through a similar mechanism as IsdH, since based on primary sequence homology it also contains the tri-domain unit that rapidly captures heme from Hb[14].

To gain insight into the mechanism of heme extraction, Gell and colleagues recently reported a 4.2 Å crystal structure of oxidized Hb in complex with the tri-domain unit from IsdH ($IsdH^{N2N3}$, residues A326-D660)[29]. In the crystal four $IsdH^{N2N3}$ proteins bind to Hb, each interacting with one of the globin chains. Each $IsdH^{N2N3}$ protein adopts an extended conformation in which its N2 domain engages the A and E helices of the globin, while the linker domain positions the N3 domain near the heme molecule that is bound to the same globin chain. Because the structure was determined at low resolution, the mechanism through which $IsdH^{N2N3}$ triggers heme release is not well understood, and the structure of the intact receptor remains unknown because the structure of the peptide segments that join the three domains could not be determined. Moreover, the structure and dynamics of the receptor in its Hb-free state have yet to be determined, so it is not known if the receptor adopts a rigid, preformed binding surface for Hb, or if its domains flexibly reorient with respect to one another prior to engaging Hb. To address these issues we used solution state NMR and small angle x-ray scattering (SAXS) data to characterize the structure and dynamics of the 38.8 kDa tri-domain $IsdH^{N2N3}$ protein in its Hb-free state, providing insight into the mechanism of heme extraction.

Results

Rate of heme transfer from Hb to $IsdH^{N2N3}$

Previous studies have shown that $IsdH^{N2N3}$ containing the N2 and N3 NEAT domains (38.8 kDa, residues A326 to D660 of IsdH) rapidly removes the oxidized form of heme (hereafter referred to as hemin) from Hb through a process that requires protein complex formation[26]. However, the rate constant describing the transfer reaction was not accurately defined because the kinetics were measured using a conventional UV-Vis instrument that failed to capture the early steps in the transfer process. To overcome this limitation we re-measured the transfer kinetics using a stopped-flow UV-Vis spectrophotometer that has a significantly shorter dead time (dead time ~3 ms versus 5 s). Upon mixing methemoglobin (metHb) with excess apo-$IsdH^{N2N3}$, a rapid shift in the UV absorbance spectrum of metHb is observed as hemin is transferred to apo-$IsdH^{N2N3}$ (Fig. 1b). Curve fitting of the time-dependent spectral changes reveals biphasic behavior with fast and slow rate constants of 0.85 ± 0.11 and 0.099 ± 0.14 s^{-1}, respectively (Fig. 1c). As a negative control similar experiments were performed using a mutant in which the linker domain is replaced with a glycine-serine nonapeptide, $IsdH^{N2\text{-}GS\text{-}N3}$. As expected, it does not acquire hemin from metHb over the timeframe of the experiment indicating the linker domain plays a critical role in hemin capture[26]. When metHb is mixed with an excess of H64Y/V68F apo-Mb as a hemin scavenging agent, the rates of simple hemin release are much slower[30] (Fig. 1d). As shown, simple thermal dissociation from metHb also shows a biphasic time course with a beta chain rate of ~ 0.003

s^{-1} and an alpha chain rate of ~0.0002 s^{-1} [28]. The fast and slow phases of hemin transfer to apo-IsdH^{N2N3} may therefore correspond to hemin removal from the beta and alpha chains of metHb, respectively. Regardless of the exact interpretation, it is clear that the receptor dramatically accelerates the rate of hemin release from the beta and alpha subunits of metHb by ~250–500 fold.

NMR relaxation measurements reveal the presence of motions between the N2 and linker domains

To investigate the mobility of the receptor we quantitatively measured ^{15}N relaxation parameters of IsdH^{N2N3} containing a Y642A mutation in the N3 domain that disrupts hemin binding. The ^{1}H-^{15}N HSQC spectrum of this protein is well resolved (Fig. 2a) and the mutation does not significantly alter the structure of the protein (not shown)[31]. Unless otherwise indicated, all NMR and SAXS studies made use of this Y642A mutant of IsdH^{N2N3}. For this protein ^{15}N spin-spin (R_2), ^{15}N spin-lattice (R_1) and {^{1}H}-^{15}N heteronuclear NOE relaxation parameters were measured for 155, 142, and 238 backbone amides, respectively (Fig. S1). The NMR relaxation data indicate that the domains within IsdH^{N2N3} predominantly tumble as a single unit in solution. Measured R_1 and R_2 relaxation rate constants indicate that IsdH^{N2N3} has a molecular correlation time (τ_c) of 16.3 ± 0.1 ns, which is very similar to the predicted τ_c value for a spherical protein of similar molecular mass (Table 1). Moreover, each of the three component domains within IsdH^{N2N3} have τ_c values that are substantially larger than values predicted for the domains if they were to tumble independently of one-another. Specifically, the N2 and N3 domains within IsdH^{N2N3} have experimental τ_c values of 13.9 ± 0.1 and 15.5 ± 0.1 ns, respectively. This indicates that they tumble as part of a larger unit, since significantly smaller τ_c values are predicted if they tumbled freely in solution. The NMR data also indicate that the intervening linker domain is part of the ordered unit that contains the N2 and N3 domains. While its τ_c value could not be reliably determined from the relaxation data because the majority of its amide bond vectors are co-linear in the structure of this module, its ^{15}N R_2 values have similar magnitudes as residues located in the surrounding N2 and N3 domains, compatible with it being part of this ordered unit.

Although the domains within IsdH^{N2N3} primarily tumble as a single unit, inter-domain motions enable the N2 domain to reorient with respect to the body of the protein. This is apparent from the experimentally determined τ_c value of the N2 domain, which is slightly smaller than the N3 domain's τ_c. The N2 domain's elevated mobility is further substantiated by the data shown in figure S1, which reveals that on average its residues have R_2 and R_1 values that are, respectively, slightly smaller and larger than residues located in the linker and N3 domains. The ability of the N2 domain to reorient is also compatible with the structure of IsdH^{N2N3} as a hydrophilic interface connects it to the linker domain (*vida infra*). Several residues connecting the domains (N465-E472 and V531-Q543) that were not determined in the crystal structure are ordered based on their relaxation data. Data for three residues located within the N2-linker connector are available for analysis (N465, D467, and V470) and are structured as they have R_2 and NOE values of 21–37 s^{-1} and 0.67–0.90, respectively. Residues within the segment connecting the linker and N3 domains are

similarly structured, as a total of 9 residues in this segment have R_2 and NOE values of 22–43 s^{-1} and 0.73–0.90, respectively.

The relaxation data also provided insight into the dynamics of the ligand binding surfaces within the N2 and N3 domains, which bind Hb and hemin, respectively. Both proteins use residues in the β7/β8 hairpin and a proximal 3_{10} helix to bind their respective ligands. Interestingly, the Hb binding surface in N2 is disordered, while the hemin binding surface in N3 is well-ordered. For example, after significant attempts were made, resonances for residues N358-D359, Q364-T370, K397-F399, A422, S439-S440, and Y451-T454 in N2 could not be assigned in the NMR spectra. These residues form the aromatic α-helix (H2) and portions of the β4, β6, β7, and β8 sheets in the Hb binding pocket, and presumably their absence in the NMR data is caused by fluctuations in their magnetic environment that occur on the micro- to millisecond time scale. In contrast, the hemin binding pocket in N3 adopts an ordered conformation in its apo-state as the backbone amide resonances of its residues could be assigned, do not exhibit significant line-broadening, and nearly all have heteronuclear NOE values greater than 0.8.

Experimental restraints used to model the structure of apo-IsdH^{N2N3}

Resonance overlap caused by the large number of residues in IsdH^{N2N3} (335 amino acids) makes it difficult to determine its structure using conventional NOE-based NMR methods. We therefore modeled the structure of the receptor using paramagnetic relaxation enhancement (PRE) derived distance restraints obtained from six single cysteine mutants of IsdH^{N2N3} that each contained a disulfide linked nitroxide spin label (R1, methanesulfonothioate)[32]. The samples have probes attached to each of the three domains: R363C (N2), E400C (N2), K499C (linker), E511C (linker), K528C (linker) and E559C (N3) (Fig. 3). Probes were attached to residues whose side chains project into the solvent in the NMR and crystal structures of the isolated domains. The backbone atoms of these residues are also structured based on their NMR relaxation data and the attached probes do not significantly alter the NMR spectra of the receptor indicating that they do not perturb the structure of the receptor. The backbone assignments of unmodified IsdH^{N2N3} have been reported previously and were used to assign the ^{1}H-^{15}N HSQC spectra of each nitroxide labeled sample recorded in its paramagnetic (oxidized) and diamagnetic (reduced) states (Fig. 2b). A comparison of the paramagnetic (I_{ox}) and diamagnetic (I_{red},) signal intensities reveal distance-dependent line-broadening of proximal amide protons. Figure 3a summarizes the PRE data for each probe showing an extended representation of IsdH^{N2N3}. Residues near each probe ($I_{ox}/I_{red} < 0.8$) are colored green, while residues separated by more than 20 Å ($I_{ox}/I_{red} \geq 0.80$) are colored red. All probes cause line-broadening in signals originating from proximal amide atoms located within the same domain. PRE-derived distance restraints were obtained as described in detail by Sattler and colleagues using an apparent molecular correlation time of 16 ns for the electron-nucleus vector[33–35]. Use of this correlation time provides good agreement with the probe-amide distances present in the known structures of the isolated domains (Fig. S2). As described by Clore and colleagues, in all calculations three conformers were used to represent the positioning of the probe to account for probe flexibility[36–38].

The PRE-derived distance restraints were supplemented with several other types of experimental data. TALOS+ was used to obtain phi and psi dihedral angle restraints for residues within the polypeptide segments that connect the domains. Two sets of $^{1}D_{HN}$ residual dipolar couplings were used as domain orientational restraints and were measured for proteins aligned in either PEG/Hexanol or *pf1* phage media. The rhombicity and magnitude of the alignment tensors were determined using the program by MODULE by best-fitting the RDC data to the known structures of the isolated N2 and N3 domains (the linker domain was not used to estimate the tensor values as its amide vectors are primarily co-linear)[39]. Several short-range NOE distance restraints were also used to define the linker-N3 domain interface and were identified by analyzing 3D ^{15}N- and ^{13}C-edited NOESY spectra recorded using a methyl selective protonated sample (U-[^{2}H], Ile-[$^{13}CH_3$ δ1], Leu, Val [$^{13}CH_3$,$^{12}CD_3$]IsdH^{N2N3}) (Fig. 2C). Finally, small angle x-ray scattering (SAXS) data was used to define the size and shape of the receptor[40].

The final model of IsdH^{N2N3} was determined using a total of 807 experimental restraints: 108 $^{1}D_{NH}$ restraints obtained using two alignment media, 629 attractive and repulsive PRE restraints, 19 NOE distance restraints, SAXS data collected in the range of $q \leq 0.3$ Å^{-1}, and 50 backbone torsion angle restraints for residues locating in the polypeptide segments that connect the domains (26 and 24 restraints for the N2-Linker and N3-linker connectors, respectively).

Structure calculation

A conjoined rigid body/torsion angle simulated annealing protocol was used to model the structure of the receptor[41,42]. In the calculation, the coordinates of the individual domains were treated as rigid bodies and are derived from the 4.2 Å crystal structure of the IsdH^{N2N3}:Hb complex (PDB code: 4IJ2). The domains were allowed to reorient with respect to one another to best-fit the experimental data by enabling the residues connecting the domains to move freely (I462-Y475 connecting the N2 and linker domains and V531-Q543 connecting the linker and N3 domains).

A multi-step calculation procedure was employed in which the N2-linker and linker-N3 inter-domain interfaces were treated separately (Fig. 4). Initially, only the structure of the interface between the linker and N3 domains was determined as it is better defined by the NOE data (a total of 1 and 7 inter-domain NOEs define the N2-linker and linker-N3 interfaces, respectively). In this calculation, residues connecting the linker and N3 domains were allowed to move freely (V531-Q543) so as to satisfy the appropriate linker-N3 inter-domain PRE, NOE, dihedral angle and RDC restraints. In addition, side chains located at this interface were allowed to move during the calculation (K488-E491, Q526-V527, S529-A530, L544, A576, Y583, K595-D596, R603, T605-S608, I619, N630, I632, K634, and Q645-H647). The SAXS data was not used in this initial calculation as it is sensitive to the global structure of the intact receptor, which is not modeled in this calculation as N2 is not considered. This calculation led to an ensemble of 20 conformers that define the relative positioning of the linker and N3 domains (step 1 in Fig. 4). The structures are compatible with the experimental data and are described in greater detail later in the text (Table 2). Next, the position of the N2 domain was determined by allowing amino acids connecting the N2

and linker domains to move freely (I462-Y475), while residues in the remainder of the protein were held rigid (atoms in the N2 domain and residues spanning the linker and N3 domains were treated as rigid bodies) (step 2 in Fig. 4). The side chains of residues at the N2-linker domain interface were also allowed to move during the calculation (N348-D353, V372-P374, T376, and N476-Q478). Conformers generated from the first set of calculations were used as input, thus the positioning of the linker and N3 domains is *a priori* well defined (Fig. 5A). These calculations generated a 'standard' single conformer depiction of the structure of the intact receptor shown in Fig. 5B (structural statistics are presented in table 3).

The NMR structure generated from the two step procedure agrees well with the experimental PRE and SAXS data. Figure 5D shows a summary of the attractive and repulsive PRE restraints demonstrating a high level of redundancy. These restraints agree well with the structure based on a violation analysis of the PRE-derived distance restraints for all of the probes versus the corresponding distance in the NMR structure (Figure S3). When the experimental error is considered, all of the PRE-derived distance restraints are satisfied to within 2.7 Å, with 98.7% of them agreeing to within 0.5 Å. Figure 6A shows a more detailed analysis of the PRE data as a function of residue number. The plots show for each probe the distance between the receptor backbone amide protons to the average position of the nitrogen atom in the spin label. There is a very good correspondence for the attractive restraints, while as expected, the repulsive restraints exhibit weaker correlation to the structure as they have no upper bound. Interestingly, a total of eight PRE-derived distance restraints are systematically violated by 0.5–2.7 Å in all conformers of the NMR ensemble. All of these restraints involve interactions with the N2 domain and suggest that this domain may undergo inter-domain rearrangements (addressed below). As expected, the NMR-derived model of apo-IsdH^{N2N3} is compatible with small angle x-ray scattering (SAXS) information as the structures were directly refined against this data (Fig. 6b). Theoretical scattering curves were generated for each member of the NMR ensemble using the program CRYSOL[43]. Individual members of the NMR ensemble fit extremely well to the solution scattering data of apo-IsdH^{N2N3} with χ values of 0.96 for the lowest energy structure. Combined, the good agreement with the PRE and SAXS data indicates that the NMR structure shown in Fig. 5b represents the predominating conformer of the receptor that exists in solution.

Model of Apo-IsdH^{N2N3}

IsdH^{N2N3} adopts an extended dumb-bell shaped structure in which the helical linker domain forms a handle that separates the N2 and N3 domains by ~23 Å (Fig. 5b). The interface between the linker and N3 domains is primarily formed by hydrophobic residues and buries ~690 Å^2 of solvent accessible surface area (Fig. 5c). At this interface, residues located at the C-terminal end of helix H3 in the linker domain pack against residues in strands β4, β5, and β7 in the N3 domain. Additional domain-domain packing interactions occur between the turn that connects the H1 and H2 helices (H1/H2 turn), and residues within strands β7 and β8 in the N3 domain. The structure of this portion of the interface is supported by inter-domain NOEs between the backbone amides of T489 and L490 located in the H1/H2 turn and the methyl group of I632 located in strand β7 (Fig. 2c). Interestingly, all of the thirteen

residues that connect the linker and N3 domains (V531-Q543) are well ordered in the NMR ensemble, whereas they were not modeled in the crystal structure of the bound protein because of the low resolution of the diffraction data. In apo-IsdH^{N2N3} they wrap around the face of the N3 domain packing against residues located in strands β2, β3, β5, and β6 in the N3 domain. While the side chain positioning for these residues is not well-defined, evidence for this interaction is provided by the NOESY data, as methyl-amide NOEs are observed between the N3 and linker domains (e.g. V537-methyl to T606-HN, V607-methyl to N541-HN and V607-methyl to D542-HN) (Fig. 2c).

In contrast to the linker-N3 interface, the contact surface between the N2 and linker domains primarily contains hydrophilic residues that bury ~550 Å^2 of solvent accessible surface area (Fig. 5c). In the IsdH^{N2N3}:Hb complex electron density for residues N465-E472 connecting the N2 and linker domains is missing. In apo-IsdH^{N2N3} these residues pack against the N-terminal end of the H1 helix within the linker domain, as well as residues located proximal to, and within, the β1a and β2 strands of the N2 domain. This connector segment is not well defined by the NOE data as the majority of its residues contain polar side chains whose proton resonances are significantly overlapped in the NOESY spectra (the N2-linker interface has only a single methyl-containing residue (V470) that exhibits an NOE to the backbone amide of Y475 located in helix H1 (Fig 2c)). Even so, the overall orientation of the domains and intervening connector are reasonably well defined by the long-range PRE data and in 75% of the conformers, interactions are observed between the ε-amino group of K391 located in the N2 domain and the hydroxyl group of Y475 located in the H1 helix of the linker domain. Additional polar interactions between the guanidino group of R350 located in the N2 domain and the side chains of N464, N465, or D468 located in the connector segment were observed in 40% of conformers.

Ensemble modeling to account for N2 domain motions

While the structure described above shown in Fig. 5b is the predominate form of the receptor in solution, it seems likely that additional, less frequently populated conformers exist in which the N2 domain adopts distinct positions relative to the linker and N3 domains. This conclusion is supported by the smaller molecular correlation time of the N2 domain compared to the remainder of the protein suggesting that it undergoes additional motions, and the fact that the single depiction of the structure results in systematic, albeit small PRE-derived distance restraint violations to the N2 domain. This notion is substantiated by an analysis of the eight violated PRE restraints. An inspection of the structure of IsdH^{N2N3} reveals that no single orientation of the N2 domain can simultaneously satisfy all of the violated restraints. This is demonstrated in Figure 7a, which shows six consistently violated PRE-derived distance restraints that originate from the E511R1, R363R1 and E559R1 probes. Violated restraints involving the R363R1 and E559R1 probes can only be satisfied by moving the N2 and N3 domains closer to together, whereas an opposing movement of the N2 domain is required to satisfy violated restraints originating from the E511R1 probe. Thus, both the NMR relaxation and PRE data suggest that the N2 domain undergoes motions that alter its poisoning relative to the remainder of the receptor resulting in a minor set of conformers that are distinct from the average conformation shown in Fig. 5b.

To gain insight into the range of conformations that are accessible to the N2 domain, a third set of calculations were performed in which the receptor was modeled as an ensemble of four molecular structures (Fig. 4, step 3). Since all of the systematically violated restraints originate from the N2 domain only the polypeptide segment that connects it to the linker domain was allowed to move, whereas residues spanning the linker and N3 domains were held rigid during the calculation. As described previously, all of the probes were modeled using three conformers and the full suite of NMR experimental data was employed. However, in the ensemble calculation four conformers were used to model the structure of the receptor and the terms of the energy potential were ensemble averaged[36]. In particular, each member of the ensemble was required to have good covalently geometries and minimal atomic overlap, whereas the entire ensemble of four molecular structures were allowed to collectively satisfy the distance, RDC and SAXS data. An ensemble size of four (Ne = 4) was used because test calculations revealed that it provided good agreement with the experimental data, whereas calculations using larger ensemble sizes resulted in minimal improvement (Fig. 7b).

The results of the Ne = 4 ensemble calculation indicate that the N2 domain can sample a range of positions relative to the linker and N3 domains that enable it to completely satisfy the PRE data. Figure 7c shows a plot of the reweighted atomic probability density map for the members of the ensemble (contoured at 10% (grey) and 50% (green) of the maximum value)[44]. Superimposed onto this map is the NMR structure of the receptor calculated assuming only a single position for the N2 domain. The density plot reveals that the N2 domain predominantly samples a narrow region of conformational space that closely matches its position in the single conformer depiction of the receptor (shaded green). In contrast, to more completely satisfy the PRE data, less frequently populated conformers exist in which the N2 adopts positions that are both closer or father away from the N3 domain.

Discussion

The bacterial pathogen *S. aureus* employs two surface receptors to capture the oxidized form of heme (hemin) from human hemoglobin (Hb), IsdB and IsdH. The receptors share extensive sequence homology over a region that contains two NEAT domains that are separated by a conserved helical “linker” domain (Fig. 1a). The N-terminal NEAT domain in each receptor binds Hb, while the C-terminal NEAT domain interacts with hemin. In IsdH, this tri-domain unit is comprised of the N2, linker, and N3 domains ($IsdH^{N2N3}$). Based on our stopped-flow hemin transfer experiments the domains in $IsdH^{N2N3}$ function synergistically, extracting hemin from Hb ~250–500 times more rapidly than the rate at which Hb spontaneously releases hemin into the solvent (Fig. 1)[26]. Previously we determined a 4.2 Å structure of the receptor bound to Hb revealing that the receptor adopts an extended structure in which the N2 domain engages the A and E helices of each globin chain enabling the linker domain to properly position the N3 domain near the hemin molecule in the same globin chain[29]. The crystal structure of the complex revealed the overall mode of binding, but it did not define the structure and dynamics of the tri-domain receptor prior to engaging Hb. We therefore used NMR spectroscopy and conjoined rigid body/torsion angle dynamics to model the solution structure of $IsdH^{N2N3}$. The NMR data

indicate that in the absence of Hb, the receptor adopts an elongated dumbbell shaped structure in which the N2 and N3 domains pack against opposite ends of the central linker domain (Fig. 5). Residues located within polypeptide segments that connect the domains that were not modeled in the low resolution structure of the $IsdH^{N2N3}$:Hb complex (PDB code: 4IJ2) are defined in the NMR model of the apo-form of the receptor and are conformationally ordered based on NMR relaxation data (Figs. 5 and S1).

In $IsdH^{N2N3}$ the N2 domain appears to undergo motions that alter its positioning relative to the linker domain, whereas the N3 domain is immobilized relative to the linker domain. These structural changes are substantiated by NMR relaxation data and the presence of two physiochemically distinct domain-domain interfaces. The linker-N3 interface is extensive and primarily hydrophobic in character with residues in the H1/H2 turn and H3 helix of the linker domain contacting residues within the β4 strand and β7/β8 hemin-binding pocket of the N3 domain. This interface is further stabilized by the polypeptide segment connecting the domains, which wraps around the body of the N3 domain making contacts to residues in strands β2, β3, β5, and β6. On the contrary, the N2-linker interface is less extensive and largely hydrophilic with only the N-terminal portion of the linker domain packing against the N2 domain. Compatible with these distinct interfaces, the NMR relaxation data indicate that the N2 domain has elevated mobility relative to the rest of the protein as it tumbles more rapidly and has shorter R2 values (Table 1 and Fig. S1). A more thorough analysis of the relaxation data is necessary to rigorously define the mobility of the N2 domain. In our analysis, fitting of R1 and R2 data yielded a slightly smaller τ_c value for N2. However, it is possible it undergoes more substantial motions. This would be the case if our R2 values were overestimated as a result of chemical exchange processes. Regardless of the degree of flexibility at the N2-linker interface, the relaxation data strongly supports the notion that the N2 domain undergoes rearrangements that move it relative to the body of the protein. Movement of the N2 domain is probably facilitated by the presence of a polar interface between it and the linker domain, whereas a hydrophobic interface between the linker and N3 domains presumably restricts inter-domain motions. N2 domain rearrangements may originate at a hinge point near residues N465-D468 that connect the N2 and linker domains, as ^{15}N relaxation analysis suggests that this is the location at which the R_1 and R_2 rates switch from N2's longer and shorter times, respectively, to the times seen throughout the linker and N3 domains.

We estimated the range of positions that are accessible to the N2 domain by performing ensemble calculations in which four molecular structures of the receptor were allowed to collectively satisfy the experimental data[36]. These calculations were performed because single conformer depictions of the receptor exhibited small, but persistent PRE-derived distance restraint violations to the more mobile N2 domain (Fig. 7a). The ensemble calculation reveals that in order to completely satisfy the PRE-derived distance restraint data the N2 domain can adopt positions that differ by as much as ~10 Å from its average position (Fig. 7c). These small excursions are compatible with our finding that the N2 domain has a smaller τ_c than the remainder of the protein and its hydrophilic interface with the linker domain. However, they presumably occur infrequently as a single depiction of the structure shown in Fig. 5b satisfies nearly all of the NMR and SAXs data. The time scale of N2 domain motions has not been defined by our analysis, but likely occurs in the nanosecond

range, since residues in the polypeptide that connect the N2 domain to the body of the protein do not exhibit substantial line-broadening and are ordered on the picosecond time scale based on their heteronuclear NOE data. Intriguingly, a proline (P466) is located at the center of this potential hinge suggesting it may be a focal point for conformational changes that reorient the domains.

The NMR data provides insight into the mobility of the hemin and Hb ligand binding pockets in the receptor. In the crystal structure of the IsdH^{N2N3}:Hb complex, residues in the H2 and H3 helices and strands β3, β6, and β7 in the N2 domain contact the A and E helices in Hb. This binding surface is unstructured and flexible in the absence of Hb, as resonances for many residues in this region are absent in the NMR spectra, presumably because they undergo micro- to milli-second motions that cause line-broadening. Specifically, resonances in the H2 helix of the N2 domain could not be assigned (Q364-T370), as well as several residues in the underlying stands β4, β6, β7, and β8 (K397-F399, A422, S439-S440, and Y451-T454). Interestingly, similar resonance line-broadening has been observed in the N1 domains from IsdB[45] and IsdH[46], which also bind Hb and like the N2 domain in IsdH^{N2N3} contain a conserved aromatic motif within the H2-helix that interacts with Hb. This suggests that like IsdH^{N2N3}, these NEAT domains also undergo a disordered to ordered transition upon binding Hb.

In contrast to the Hb binding pocket in the N2 domain, the backbone atoms of residues in the hemin binding pocket in the N3 domain are generally inflexible in the absence of hemin based on the observation that their backbone amide atoms could be assigned in the NMR spectra and their heteronuclear NOE values and R_2 relaxation parameters. Notably, the relaxation data indicate that residues connecting strands β7 and β8 that form one face of the hemin pocket are semi-ordered in the absence of hemin (V637-E645). In particular, the amide cross-peaks of residues A638 and I640-E645 are not significantly broadened in the NMR data, have R_2 values near the average for the core of the N3 domain, and have heteronuclear NOE values > 0.5. Interestingly, many of these residues are absent in the electron density for two out of three N3 domains in the 4IJ2 crystal structure. Their absence may be caused by static disorder in the crystal as hemin derived from denatured Hb in the crystallization drop was proposed to partially occupy the binding site in N3. This notion is compatible with structural studies of the isolated N3 domain which show that hemin binding causes a small shift in the conformation of this hairpin which is otherwise conformationally ordered [47].

A comparison of the NMR model of the average structure of IsdH^{N2N3} with the structure of the receptor in the IsdH^{N2N3}:Hb complex reveals that Hb binding repositions the N2 domain (Fig. 8). As compared to the NMR structure of the apo-form of the protein, the receptor in the crystal structure of the complex is more compact as a result of a ~30° rotation that moves it ~7 Å towards the N3 domain. This structural difference is substantiated by PRE-derived distance restraints obtained from the R363R1 and E511R1 samples, which are incompatible with the conformation of the bound receptor observed in the crystal structure (Fig. 3b). For example, the PRE data indicate that the E511R1 probe located in the N-terminal portion of helix H3 in the linker domain is within ~15–20 Å of the backbone amide hydrogen atoms of several residues located within the N2-linker interface (H344, N348, V372, T376, I379-

F379, E387) as their resonances are substantially broadened by the probe (I_{ox}/I_{red} ratios ~0.3–0.7) (Fig. 3b). In contrast, modeling studies using the crystal structure indicate that the E511R1 probe would be separated from these residues by at least 27 Å. Data derived from the R363R1 probe attached to the N2 are also incompatible with the crystal structure; the probe is at least 20 Å away from the backbone amides of F555, E562, S563, V628-N630, and V648-N652 located in the N3 domain of apo-IsdH^{N2N3} as supported by I_{ox}/I_{red} values greater than 0.9, but in the crystal structure they are closer than this distance. While the positioning of the N2 domain is different between the bound and unbound states of IsdH^{N2N3}, not surprisingly the relative domain orientation at the extensive hydrophobic linker-N3 interface is largely unaffected by Hb binding, suggesting that this portion of the receptor moves as a rigid unit in solution. The incompatibility of the PRE data with the crystal structure of the receptor is solely due to differences in domain positioning as only these types of long-range distance restraints were used in our calculations. Interestingly, the structural differences in the N2 domain supported by the PRE data are not distinguished by the SAXS data. This result is demonstrated in Fig. 6a and 6b, which shows excellent agreement between the SAXS data and the coordinates of the free and bound forms of IsdH^{N2N3}, respectively (the χ values of the NMR and crystal structures are 0.96 and 0.92, respectively).

It seems likely that receptor binding to Hb occurs through a combination of ‘induced fit’ and ‘conformational selection’ mechanisms. The results of the Ne = 4 ensemble calculation provide strong evidence that Hb binding in part occurs through ‘conformational selection’ in which Hb selects from among different forms of the receptor a binding competent conformer. This idea is evident in Fig. 7d, which displays the reweighted atomic probability density map of apo-IsdH^{N2N3} superimposed onto the crystal structure of the receptor in the IsdH^{N2N3}:Hb complex. The plot reveals that in the absence of Hb, the receptor may infrequently sample conformers that resemble its Hb-bound form in which the N2 and N3 domains are more closely positioned (Fig. 8). However, as described above, the predominating form of the receptor in solution adopts a more open state in which the N2 domain is displaced from the N3 domain as a significant portion of the crystal structure resides outside the highly populated region of the density map (shaded green).

Receptor binding to Hb presumably must also occur through an induced fit mechanism in order to explain how the receptor captures hemin from Hb ~250–500 times faster than the rate at which Hb spontaneously releases hemin into the solvent (Figs. 1c versus 1d). To promote hemin release, the receptor must destabilize Hb-hemin interactions. Our single conformer model of the receptor (Fig. 5b), in combination with the crystal structure of the complex, suggests how the receptor might transiently induce structural changes in Hb that promote hemin release. A model of Hb bound to the structure of IsdH^{N2N3} determined by NMR (called ^{NMR}IsdH^{N2N3}:Hb) was generated by superimposing the coordinates of the N2 domain in the NMR model of IsdH^{N2N3} onto the corresponding coordinates in the crystal structure of the IsdH^{N2N3}:Hb complex (Fig. 9). The modeled structure of ^{NMR}IsdH^{N2N3}:Hb may represent the initial binding of Hb to the receptor prior to it rearranging through N2 domain motions into the more stable structure visualized by x-ray crystallography. As seen in the ^{NMR}IsdH^{N2N3}:Hb model, initial binding of the apo-receptor to Hb results in atomic overlap between residues in the F-helix and C-terminus of αHb (A79, N78, S81, D85, and

Y140) and residues in the H1 and H2 helices of the linker domain (K479, K486, R492, E496, K499, and K503). Similar atomic overlap is seen when the apo-receptor is docked to Hb's beta subunit (model not shown). We speculate that these receptor-Hb interactions may promote hemin release by altering the positioning of the F-helix which houses the proximal histidine that coordinates the iron in hemin (H87 in the alpha subunits and H92 in the beta subunits, which is conventionally referred to as HisF8). Although details of this process are not known, this transient distortion in Hb may increase fluctuations in the proximal pocket area that facilitate water penetration needed to break the Fe-HisF8 bonds in both subunits. The receptor would then undergo a structural transition about the N2-linker interface so as to adopt the more stable conformation observed in the 4.2 Å crystal structure of the $IsdH^{N2N3}$:Hb complex (Fig. 8)[29].

Receptor mediated transient distortion of Hb may also explain recent mass spectrometry results, which demonstrated that a hemin-binding impaired receptor can nevertheless promote Hb tetramer dissociation[26]. In principle, receptor binding to Hb could also accelerate hemin transfer by increasing the effective concentration of the N3 domain near Hb's bound hemin molecule. However, this effect is expected to be small as the rate of hemin transfer exhibits a hyperbolic dependence on the concentration of the receptor (data not shown), compatible with the rate limiting step in the transfer reaction being breakage of the Fe-HisF8 bond in Hb. Based on the ensemble calculations Hb may also bind to other, more sparsely populated conformers of the receptor ('conformational selection') that could also induce transient structural changes in the F-helix to promote hemin release. This idea is intriguing, as it suggests that the plasticity of the N2-linker interface is critical for function. If the interface is too flexible, binding would occur solely through the conformational selection process and would presumably not alter Hb-hemin interactions needed to promote hemin release. In contrast, if the N2-linker interface was stabilized by extensive inter-domain interactions and therefore too structurally rigid, binding to Hb would be impaired as a result of sustained atomic overlap with the F-helix.

The *S. aureus* IsdB protein presumably extracts hemin from Hb through a similar mechanism as described here for $IsdH^{N2N3}$ because the proteins share 48% primary sequence identity, and similar to $IsdH^{N2N3}$, the IsdB protein extracts hemin using functionally and structurally homologous NEAT domains that are separated by a helical linker segment. Recent results reported independently by the Lei and Murphy groups further support mechanistic similarity between the two Hb receptors as they imply that the linker domain in IsdB plays an important role in Hb binding and hemin capture[45,48,49]. This is consistent with our proposal that the related region in $IsdH^{N2N3}$ may transiently interact with Hb to destabilize the F-helix that interacts with hemin. It will be interesting to discover if similar to $IsdH^{N2N3}$, the Hb binding NEAT domain in IsdB also undergoes domain rearrangements upon binding Hb. This would appear to be the case as recently reported NMR studies of the Hb binding NEAT domain in IsdB suggest that it does not significantly interact with the linker domain in the absence of Hb[45].

It is also possible that IsdB and IsdH may not use identical mechanisms to extract hemin from Hb. The Lei group showed that a ~85 residue segment preceding the Hb-binding domain (called the NS in their study) is important for the rapid kinetics observed in the

hemin transfer reaction between metHb and IsdB. It is unclear if residues preceding IsdH's Hb-binding N1 and N2 domains share a similar function as the NS in IsdB. Furthermore, recent reports[48,49] have independently shown that IsdB constructs containing the Hb binding N1 domain and the analogous linker domain could bind Hb and promote hemin transfer to the isolated hemin binding N2 domain when provided *in trans*. This finding is in contrast to IsdH, where all three domains must be within the same polypeptide for rapid hemin transfer from metHb[26]. The origin of this difference needs to be resolved, but could be caused by non-covalent interactions between Hb and the hemin-binding domain and/or the linker domain, which are not present in $IsdH^{N2N3}$. In order to elucidate mechanistic differences between IsdB and IsdH, the structure of the IsdB in its Hb-free and -bound state will need to be determined.

In summary, our NMR results in combination with the recently determined crystal structure of the Isd^{N2N3}:Hb complex suggest that the receptor may accelerate hemin release from Hb by transiently contacting Hb's F-helix. A generally similar mechanism may also be used by IsdB based on primary sequence homology and recent biochemical studies. Many other Gram-positive microbes use NEAT containing proteins to acquire heme from Hb[24]. How these proteins operate to capture heme is only beginning to be elucidated, and is important, as it could lead to development of broad-spectrum anti-infective agents that target nutrient acquisition.

Material and Methods

Protein production for NMR studies

Two IsdH polypeptides were characterized by NMR: (1) $IsdH^{N2N3(Y642A)}$, which contains N2, linker and N3 domains (residues A326-D660) and a Y642A mutation in the hemin pocket of $IsdH^{N3}$ domain that disrupts hemin binding and (2) $IsdH^{N2\text{-}Linker}$, which contains the N2 and linker domains (residues A326-Q543). As described previously, both polypeptides were produced from pET-28b-based expression plasmids and initially contained a removable N-terminal hexahistidine-small-ubiquitin-like modifier (SUMO) tag to facilitate purification[50,51]. Several uniformly isotopically labeled samples were produced for NMR studies using *Escherichia coli* BL21 (DE3) cells (New England BioLabs, Beverly, MA). Uniformly isotopically labeled proteins were expressed from cells grown in M9 minimal media containing 2 g/L [^{13}C]-glucose and/or 1 g/L $^{15}NH_4Cl$ as the sole source of carbon and nitrogen, respectively (Cambridge Isotope Laboratories, Andover, MA). The methods to overexpress the proteins have been described previously[26,31]. Briefly, expression proceeded overnight at 25°C by adding 1 mM isopropyl-β-D-thiogalactoside to cell cultures. The bacterial cells were then harvested by centrifugation, lysed by sonication, and the protein was purified using a Co^{2+}-chelating column (Thermo Scientific, Waltham, MA). The amino terminal 6x-His-SUMO tag was then cleaved using ULP1 protease and reapplied to the Co^{2+}-chelating column to remove the protease and cleaved SUMO tag. The final protein yield for U-[^{13}C,^{15}N]$IsdH^{N2N3(Y642A)}$ and U-[^{13}C,^{15}N]$IsdH^{N2\text{-}Linker}$ was 21 mg/L and 14 mg/L, respectively. Methods used to produce the U[^{2}H,^{13}C,^{15}N]$IsdH^{N2N3(Y642A)}$ NMR sample have been described previously[31]. The protocol used to produce the methyl protonated U-[^{2}H], Ile-[$^{13}CH_3$ δ1], Leu, Val-[$^{13}CH_3$,$^{12}CD_3$] $IsdH^{N2N3(Y642A)}$ sample is

similar to the protocol used to produce the U-[^{2}H,^{13}C,^{15}N]IsdH$^{N2N3(Y642A)}$ sample. However, 3 g/L of U-[^{13}C, ^{2}H]-glucose (Isotec, Miamisburg, OH) was used as the carbon source, as well as one hour prior to induction 60 mg/L of [U-$^{13}C_4$, 3,3-$^{2}H_2$]-α-ketobutyrate (Cambridge Isotope Laboratories, Andover, MA) and 100 mg/L of [1,2,3,4-$^{13}C_4$, 3,4′,4′, 4′-$^{2}H_4$]-α-ketoisovalerate (Cambridge Isotope Laboratories, Andover, MA) were added to the growth medium to yield 33 mg/L culture. All NMR samples were dissolved in NMR buffer containing 20 mM NaH_2PO_4, 50 mM NaCl, 0.01% NaN_3, pH 6.0 supplemented with ~8% D_2O. The following samples were used for NMR studies: 1.1 mM U-[^{2}H, ^{13}C,^{15}N]IsdH$^{N2N3(Y642A)}$, 1.0 mM U[^{13}C,^{15}N]IsdH$^{N2N3(Y642A)}$, 0.8 mM U-[^{2}H], Ile-[$^{13}CH_3$ δ1], Leu, Val-[$^{13}CH_3$,$^{12}CD_3$]IsdH$^{N2N3(Y642A)}$, 0.675 mM U-[^{13}C,^{15}N]IsdH$^{N2\text{-}Linker}$, and two additional samples of 1.2 mM U-[^{13}C,^{15}N]IsdH$^{N2N3(Y642A)}$ and 1.2 mM U-[^{13}C,^{15}N]IsdH$^{N2\text{-}Linker}$, both lyophilized in NMR buffer and resolublized with an equal volume of 99.999% D_2O (Isotec, Miamisburg, OH).

PRE measurements were made using four double mutants of IsdH^{N2N3}. Each mutant contained the Y642A mutation that disrupts hemin binding as well as a single cysteine mutation at the following residues: R363C, E400C, K499C, E511C, K528C, and E559C. Expression plasmids producing the mutant proteins were obtained by site directed mutagenesis of plasmid pRM216 that produces IsdH$^{N2N3(Y642A)}$ with a N-terminal hexahistidine-small-ubiquitin-like modifier (SUMO) tag (QuikChange Site-Directed Mutagenesis Kit, Stratagene, La Jolla, CA). For NMR studies uniformly ^{15}N labeled samples of each protein were produced in an identical manner as describe above, with the exception that 2.5 mM dithiothreitol (DTT) was added to all buffers used during the purification procedure. After purification and protein concentration, the sampled was dialyzed against labeling buffer (50 mM Tris, 50 mM NaCl, 2.5 mM DTT, pH 7.8). The DTT was then removed using a desalting column (Zeba Spin Desalting Column, Thermo Scientific, Waltham, MA). Probes were attached to each sample by immediately incubating them with a ten-fold molar excess of methanesulfonothioate (MTSL; Toronto Research Chemicals, North York, ON, CAN) for 15 minutes, after which an additional ten-fold molar excess of MTSL was added followed by incubation overnight at room temperature. Disulfide bond formation between MTSL and the sulfhydryl group of the cysteine was confirmed via MALDI-TOF and any unreacted MTSL was removed by buffer exchange (Amicon centrifugation filtration device, Millipore, Billerica, MA) with NMR buffer. For PRE measurements, each U-[^{15}N]-labeled cysteine mutant (IsdH$^{R363C(Y642A)}$, IsdH$^{E400C(Y642A)}$, IsdH$^{K499C(Y642A)}$, IsdH$^{E511C(Y642A)}$, IsdH$^{K528C(Y642A)}$, and IsdH$^{E559C(Y642A)}$) was concentrated to ~0.3 mM to prevent non-specific intermolecular effects.

Hemin transfer experiments

Purified unlabeled IsdH^{N2N3} and IsdH$^{N2\text{-}GS\text{-}N3}$ in which the linker was replaced with a nine-amino acid artificial linker (GSGSGSGSG) was produced as previously described[26]. The apo-form of IsdH^{N2N3} was generated by hemin extraction with methyl ethyl ketone[52] followed by buffer exchange into phosphate buffered saline solution, pH 7.4. Native human hemoglobin (Hb) was prepared in a complex with CO, as previously described[53]. Replacement of the bound CO by O_2 was accomplished by equilibrating the HbCO solution with 1 atm O_2, on ice, under light in a rotary evaporator. Methemoglobin (metHb) was

produced by incubating the oxyhemoglobin complex with excess potassium ferricyanide and loading the sample onto a G-25 sepharose column to remove excess ferricyanide[14]. metHb was then buffer exchanged into phosphate buffered saline solution, pH 7.4. The concentration of hemin within metHb was determined using the extinction coefficient of 179 $mM^{-1}cm^{-1}$[54]. The rates of hemin transfer from metHb (hemin donor) to the hemin acceptors were measured using an OLIS RSM1000 stopped-flow spectrophotometer (OLIS, Bolgart, GA) at Rice University as previously described[55,56]. Holo-protein (HbA) in one syringe was mixed with apo-acceptor at ~4x molar excess in another syringe. The entire spectrum was recorded over 300 seconds with a dead time of ~3ms. The absorbance changes at 370 and 404 nm ($\Delta A_{404-370}$)[26] were fitted to a double phase exponential expression to obtain the apparent rate constants for the transfer reaction using GraphPad Prism version 5.01 for Windows (GraphPad Software, La Jolla, CA). The rates of hemin transfer from metHb to H64Y/V68F apo-Mb[30] in ~16x molar excess was measured using a conventional UV-vis spectrophotometer (Cary50, Varian, Inc., Palo Alto, CA) also at Rice University. The entire spectrum was recorded over 790 min and the absorbance change at 409 nm was fitted to a double phase exponential equation.

NMR data acquisition

NMR spectra were acquired at 310 K for $IsdH^{N2N3(Y642A)}$ and 323 K for $IsdH^{N2\text{-}Linker}$ on Bruker Avance 500-, 600-, and 800-MHz spectrometers equipped with triple resonance cryogenic probes. All NMR spectra were processed using NMRPipe[57] and analyzed using CARA (version 1.8.4)[58] and/or SPARKY[59] software packages. Chemical shift assignments (^{1}H, ^{13}C, ^{15}N) for the backbone of $IsdH^{N2N3(Y642A)}$ have been described earlier[31]. Backbone assignments for the U-[^{13}C,^{15}N]$IsdH^{N2\text{-}Linker}$ protein were obtained by analyzing the following experiments: HNCACB, CBCA(CO)NH, HNCO, HN(CA)CO, and CC(CO)NH[60]. Side chain assignments were obtained by analyzing HNHA, HNHB, HBHA(CO)NH, (h)CCH-TOCSY, HCCH-TOCSY, and HCCH-COSY spectra acquired using U-[^{13}C,^{15}N]$IsdH^{N2N3(Y642A)}$ and U[^{13}C,^{15}N]$IsdH^{N2\text{-}Linker}$ samples. The majority of methyl resonance assignments were obtained by analyzing the following NMR spectra acquired using the methyl protonated sample: (1) ^{15}N-edited TROSY-NOESY (200 ms mixing time; collected with 2048, 64, and 160 complex points for the direct ^{1}H, ^{15}N, and indirect ^{1}H dimensions, respectively, and processed to a digital resolution of 0.09 ppm, 0.11 Hz, and 0.03 ppm for direct ^{1}H, ^{15}N, and indirect ^{1}H dimensions, respectively), (2) ^{13}C-edited NOESY in H_2O (200 ms mixing time; acquired with 2048, 76, and 244 complex points for the direct ^{1}H, ^{13}C, and indirect ^{1}H dimensions, respectively, and processed to a digital resolution of 0.14 ppm, 0.08 ppm, and 0.04 ppm for direct ^{1}H, ^{13}C, and indirect ^{1}H dimensions, respectively), (3) (h)CCH-TOCSY, and (4) CC(CO)NH experiments[60].

$^{1}D_{NH}$ residual dipolar couplings were measured on protein samples partially aligned in either 5% PEG $C_{12}E_5$/hexanol[61] or 9 mg/mL *pf1* phages[62] (ASLA Biotech, Latvia). Two-dimensional ^{15}N-coupled IPAP ^{1}H-^{15}N HSQC[63] spectra were collected for both aligned and unaligned samples (collected with 2048, and 1200 complex points for the ^{1}H, and ^{15}N dimensions, respectively, and processed to a digital resolution of ~0.21 ppm for the ^{1}H and ~0.90 ppm for the ^{15}N dimensions). ^{15}N–^{1}H 2D TROSY-HSQC spectra were recorded for each PRE spin-labeled mutant (collected with 2048 and 256 complex points for the ^{1}H,

and ^{15}N dimensions, respectively, and processed to a digital resolution of ~0.25 ppm for both ^{1}H and ^{15}N dimensions). After data acquisition for the paramagnetic samples was completed, ascorbic acid (5-fold molar excess relative to MTSL concentration) was added to the NMR tube to generate the diamagnetic sample, followed by a three-hour incubation period in the spectrometer before to acquiring the diamagnetic spectra.

^{15}N relaxation data (T1 and T2) and heteronuclear {^{1}H}-^{15}N NOE data was collected on Bruker Avance 800-MHz spectrometer equipped with a triple resonance cryogenic probe at protein concentrations of 1.9 mM for T1 and T2 relaxation experiments and 1.1 mM for heteronuclear NOE experiments. Delays used for T1 experiments were 41, 165, 393, 662, 848, and 1219 ms. For T2 experiments the delays were 17, 34, 51, 68, 85, and 118 ms. The heteronuclear NOE experiments were collected in duplicate with a relaxation delay of 5 s. Data was analyzed in SPARKY[59] to generate raw relaxation and NOE parameters.

RDC, dihedral angle, SAXS and NOE distance restraints

$^{1}D_{NH}$ couplings for 40 and 68 residues were obtained for the protein aligned in 5 % PEG/Hexanol and 9 mg/mL *pf1* phages, respectively. Data were analyzed using the program MODULE[39] to determine magnitude of the alignment tensor (D_a) and rhombicity (η). For the PEG/Hexanol data D_a and η values of 16.9 Hz and 0.21 were obtained, respectively. For the phage data D_a and η values of 10.9 Hz and 0.24 were obtained, respectively. Couplings were obtained by analyzing IPAP experiment data of unaligned and aligned samples using the published backbone chemical shifts of IsdH[31]. For both media, couplings were obtained for each of the three domains. An analysis of the euler angles of the alignment tensors revealed that they were not co-linear and aligned the protein to differing extents. The program TALOS+[64] was used to obtain phi and psi dihedral angle restraints from backbone chemical shift assignments for the loop regions between N2-Linker (residues I462-Y475) and Linker-N3 (residues A530-L544) as well as residues Y629-I650 in the hemin binding pocket of N3. Methyl side chain resonances were assigned by analyzing ^{15}N-NOESY, ^{13}C-NOESY (in H_2O), and CC(CO)NH spectra of this sample. In addition, limited side chain assignments for non-methyl side chains were obtained using a ^{13}C, ^{15}N labeled sample of IsdH$^{N2N3(Y642A)}$ and data from HCCH-COSY, HCCH-TOCSY, and (h)CCH-TOCSY spectra obtained using a ^{13}C, ^{15}N labeled sample of IsdH$^{N2N3(Y642A)}$. An analysis of the 3D-^{15}N-edited and ^{13}C-edited NOESY spectra of the selectively protonated samples identified a total of 1 and 8 inter-domain proton-proton NOEs that define the N2-linker and linker-N3 interfaces, respectively. A total of 8 hydrogen bond distance restraints for residues Y475-K479 and V531-E535 were included in the calculations and were based on alpha-helical NOE patterns observed in the ^{15}N-edited NOESY spectrum and TALOS+ calculated dihedral angles. Small angle x-ray scattering (SAXS) data for IsdH$^{N2N3(Y642A)}$ was collected using an Anton Paar SAXSess instrument with a sealed tube source. *I*(0) values and *P(r)* curves were calculated using GIFT (Anton Paar, Graz, Austria) and PRIMUS[29,65].

PRE-derived distance restraints

PRE-derived distance restraints were made for each cysteine mutant of U-[^{15}N] IsdH$^{N2N3(Y642A)}$ which contained an attached MTSL nitroxide spin label: IsdH$^{R363C(Y642A)}$, IsdH$^{E400C(Y642A)}$ IsdH$^{K499C(Y642A)}$, IsdH$^{E511C(Y642A)}$, IsdH$^{K528C(Y642A)}$, and

IsdH$^{E559C(Y642A)}$. The procedure used to analyze the PRE data is similar to the method described Sattler and colleagues[33,34,37,66–71]. The PRE effect on the transverse relaxation rate of the amide proton, R_2^{sp}, was back calculated from the ratio of peak intensities for the paramagnetic (I_{ox}) and reduced diamagnetic (I_{red}) using equation 1

$$\frac{I_{ox}}{I_{red}} = \frac{R_2 \, e^{-R_2^{sp} t}}{R_2 + R_2^{sp}} \quad (1)$$

where R_2 is intrinsic amide proton transverse relaxation rate, and t is the total INEPT evolution time recorded (11 ms). The fitted PRE rate enhancements (R_2^{sp}) were converted into distances, r, using a modified version of the Solomon-Bloembergen in equation 2[66,72]

$$r = \left[\frac{K}{R_2^{sp}} \left(4\tau_C + \frac{3\tau_C}{1+\omega_h^2 \tau_C^2} \right) \right]^{1/6} \quad (2)$$

where K is a constant (1.23×10^{-32} cm^6 s^{-2}) that describes the spin properties of the MTSL spin label[66], ω_h is the Larmor frequency of the proton spin, and τ_C is the apparent PRE correlation time[33]. The value for τ_C was estimated by comparing the agreement between distances calculated from the PRE data with known intra-domain distances present in the structures of the isolated domains (Fig. S2) (PDB code: 4IJ2). To prevent over estimation of PREs, only residues with {^{1}H}-^{15}N NOE values > 0.6 and isolated ^{1}H-^{15}N cross-peaks in the spectra were used to obtain PRE-derived restraints. Intensity ratios were normalized from the average ratios of intra-domain backbone amides known to be ≥ 28 Å away from the probe based on the NMR and crystal structures of the isolated domains. In the structure calculations, two types of distance restraints were employed: (1) attractive restraints between the nitrogen atom of the MTSL ring and affected amide proton if I_{ox}/I_{red} was < 0.80. The distance restraint for these interactions was determined using equation 2 assuming an error of ± 5 Å (2) repulsive restraints were used if $I_{ox}/I_{red} \geq 0.80$. For these amide-probe interactions a lower bound distance of 20 Å was employed and contained no upper bound[66,69,73]. Notably, all six probes caused modest line-broadening in residues within the ligand binding pockets of the N2 and N3 NEAT domains. These interactions were deemed to be non-specific because both binding pockets contain a large number of aromatic residues that are expected to non-specifically interact with MTSL[66,74]. In addition, the interactions are incompatible with all of the other PRE-derived distance restraints and SAXS data. Moreover, many of the effected residues have {^{1}H}-^{15}N NOE values < 0.6. It should be noted that the probe located in the N3 domain, E559R1, also displayed non-specific effects to a portion of N2 domain near the N-terminus. Those residues were also omitted from the calculations for the aforementioned reasons, and because data collected on an additional probe near the N-terminus, E343R1, did not display the reciprocal effect.

Relaxation data analysis

NMR relaxation data for individual residues were interpreted as described previously[75,76]. Briefly, the program Pdbinertia was used to calculate the principal moments of inertia for the NMR model of IsdHN^{2N3} yielding relative moments of inertia of 1.0:0.94:0.25. The

program R2R1_tm was used to calculate an approximate correlation times (τ_m) on a per residue basis using R_2/R_1 ratios. Only R_2/R_1 ratios that met the following criteria were used in this analysis: (1) they were from isolated ^{1}H-^{15}N cross-peaks in each spectrum 2) they were within two standard deviations of the average and (3) the residue had a {^{1}H}-^{15}N NOE value > 0.6. The data was then inputted into the program Quadric_Diffusion[77,78], which indicated that the axially symmetric model statistically is preferred over the isotropic and anisotropic models of tumbling for the intact receptor and for every subdomain with the exception of the linker that favored isotropic model. NMR relaxation data were also interpreted to obtain the diffusion tensors and molecular correlation times of the individual subdomains. For this analysis NMR data for 52, 10, and 29 residues in the N2, linker and N3 domains were used, respectively. These residues, in addition to meeting the R_2/R_1 criteria described above, were present in the electron density map of the crystal structure. Relaxation data were collecting using a 1.9 mM U[^{15}N]IsdH$^{N2N3(Y642A)}$ dissolved in NMR buffer containing 20 mM NaH_2PO_4, 50 mM NaCl, 0.01% NaN_3, pH 6.0 supplemented with ~8% D_2O. The protein is monomeric based on size exclusion chromatography combined with multi angle light scattering (SEC-MALS).

Structure calculations

Structures were calculated using XPLOR-NIH (version 2.37)[79]. The coordinates of the N2, linker and N3 domains are derived from the 4.2 Å crystal structure of the IsdH^{N2N3}:Hb complex (PDB code: 4IJ2, chain G). Polypeptide segments connecting these subdomains (N465-E472 and V531-Q543) were added using the program COOT[80]. Because they are absent in the crystal structure of the IsdH^{N2N3}:Hb complex, the coordinates for residues in the hemin-binding region of the receptor (V635-Q645) were modeled using the previously reported structure of the isolated N3 domain[47] (PDB code: 2Z6F), except that an alanine was substituted at position Y642. Protons were then added to the starting model using http://spin.niddk.nih.gov/bax/nmrserver/pdbutil and the coordinates were energy minimized. Three conformers of each MTSL probe were then added to each of the six aforementioned probe attachment sites. The coordinates of each sub-domain in the MTSL-conjugated starting structure were energy minimized against the appropriate RDC data to optimize their agreement, and to improve covalent geometry and atomic overlap. Three distinct conjoined rigid body/torsion angle simulated annealing calculations were performed (summarized in Fig. 4). In the first calculation, the coordinates of the linker and N3 domains were held rigid, but allowed to move with respect to one another so as to satisfy the relevant RDC, dihedral angle, NOE, and PRE data. In this process the coordinates of residues connecting the domains (V531-Q543) were allowed to move freely as well as the coordinates of side chains that reside at the linker-N3 interface (K488-E491, Q526-V527, S529-A530, L544, A576, Y583, K595-D596, R603, T605-S608, I619, N630, I632, K634, Q645-H647). Both the NOE data and the results of initial structure calculations indicate that the packing between the H1/H2 turn in the linker domain and N3 domain are similar in the Hb-free and -bound forms of the receptor. The posDiffPotTool module in XPLOR-NIH was therefore employed to define this region. The statistics describing the results of the first calculation are presented in Table 2. The structures generated from the first calculation were used as input into a second set of calculations. In this calculation the coordinates the appropriate position of the N2 domain was determined. The coordinates of the N2 domain and residues spanning from the

linker domain to end of the protein (N476-I655) were treated as rigid bodies. These segments were allowed to reorient with respect one another by allowing free movement of residues I462-Y475 that connect the N2 and linker domains. In addition, the coordinates for side chains of inter-facial residues (N348-D353, V372-P374, T376, and N476-Q478) were given full degrees of freedom. All of the experimental data was employed in this calculation, including SAXS data. The calculation resulted in single conformer representations of the structure that best satisfy the experimental data (statistics described in Table 3).

In the third set of calculations an ensemble approach was used to account for domain motions. This calculation is nearly identical to calculation #2, except that four conformers of the receptor (Ne = 4) were used to collectively satisfy the NMR data [36]. In particular, each member of the Ne = 4 ensemble was required to have good covalently geometries and minimal atomic overlap, whereas the entire ensemble of four molecular structures were allowed to collectively satisfy the distance, RDC and SAXS data. The RAPPot potential in the posRMSDPotTools module in XPLOR-NIH was used to minimize the spread of the atomic coordinates[81]. A total of 100 four-member ensembles were calculated. The five lowest energy ensembles (20 structures total) were used to calculate a reweighted atomic probability density map using the program VMD-Xplor[44,82].

The following parameters were employed in each of the three calculations. Initially, a total of 5000 steps of higher energy dynamics at 3500K was performed, followed by 100 cooling cycles in which the bath temperature was decreased from 3500K to 25 K in 12.5 K increments. This was followed by 5 rounds of 500 steps of Cartesian coordinate energy minimization. The final force constants used during simulated annealing for RDC, NOE, and dihedral angle (CDIH) potentials were 1.5 kcal mol^{-1} Hz^{-2}, 30 kcal mol^{-1} $Å^{-2}$, and 400 kcal mol^{-1} rad^{-2}, respectively. The non-bonded interactions were described by a van der Waals repulsion term with a final force constant of 4 kcal mol^{-1} $Å^{-2}$ and a scale factor of 0.8. A multi-dimensional torsion angle database of mean force (RAMA) potential was applied with a final force constant of 1 kcal mol^{-1}. The bond length (BOND), bond angle (ANGL) and improper dihedral (IMPR) potentials employed force constants of 1 kcal $mol^{-1}Å^{-2}$, 1 kcal $mol^{-1}rad^{-2}$, and 1 kcal $mol^{-1}rad^{-2}$, respectively. All dynamics and minimization steps utilized the internal variable module (IVM)[81,83–86]. In the single conformer calculations (calculations #1 and #2), the D_a and rhombicity of the two alignment tensors for the RDC data were held fixed during the simulated annealing, and allowed to float during the Cartesian coordinate energy minimization. In the third calculation the alignment tensor parameters were fixed throughout the calculation as to not over-fit the RDC data[40,87]. Calculations that included the N2 domain (#2 and #3) used SAXS data collected in the range of $q \leq 0.3$ $Å^{-1}$. The xray force constant was optimized such that the resulting χ^2 values were less than one, without causing violations of other restraints (final force constants of 200 and 40 kcal mol^{-1} for calculation #2 and #3, respectively [40]. Structural models were inspected and visualized using the programs MOLMOL[88] and PyMOL[89].

For the PRE data a quality factor, *Q*, was calculated using equation 3

$$Q=\sqrt{\frac{\sum(V_{backcalc}-V_{exp})^2}{\sum(V_{exp})^2}} \quad (3)$$

where $V_{backcalc}$ *and* V_{exp} are the back calculated and experimental I_{ox}/I_{red} ratios for a given spin label. This equation has been described previously[33,37] and is a modified version of the PRE *Q*-factor used in previous studies, which employs peak intensity ratios in place of enhanced relaxation rates[36,66]. The individual members within the final ensemble of back calculated scattering curves were fit to the experimental data using both the CalcSAXS helper program in the XPLOR-NIH structure determination package (v. 2.37)[40,79] as well as the program CYSOL[43].

Supplementary Material

Refer to Web version on PubMed Central for supplementary material.

Acknowledgments

We thank members of the Clubb lab for useful discussions, Dr. Robert Peterson for assistance with the NMR experiments, and Dr. Duilio Cascio for assistance in generating the starting structure. We also appreciate the comments of the reviewers who helped us significantly improve this manuscript. This work was supported by National Institutes of Health Grants AI52217 (to R.T.C.), P01-HL110900 (to J.S.O.), the Robert A. Welch Foundation Grant C-0612 (to J.S.O.), and the National Institutes of Health Award F31GM101931 (to M.S.). The chemical shift assignments, residual dipolar couplings, and relaxation data have been deposited at the BioMagResBank (http://www.bmrb.wisc.edu) under accession number 25113.

Abbreviations

Hb	hemoglobin
Isd	iron-regulated surface determinant
NEAT	near iron transporter
NMR	nuclear magnetic resonance
PRE	paramagnetic relaxation enhancement
RDC	residual dipolar coupling
MTSL	methanesulfonothioate
HSQC	heteronuclear single quantum coherence
NOE	nuclear Overhauser effect
SAXS	small angle x-ray scattering
RMSD	root mean squared deviation
Mb	Myoglobin

References

1. Klevens RM, Morrison MA, Nadle J, Petit S, Gershman K, Ray S, Harrison LH, Lynfield R, Dumyati G, Townes JM, Craig AS, Zell ER, Fosheim GE, McDougal LK, Carey RB, Fridkin SK.

Invasive methicillin-resistant Staphylococcus aureus infections in the United States. JAMA. 2007; 298:1763–71. [PubMed: 17940231]

2. Centers for Disease Control and Prevention. Active Bacterial Core Surveillance Report, Emerging Infections Program Network, Methicillin- Resistant Staphylococcus aureus. 2011. at <http://www.cdc.gov/abcs/reports-findings/survreports/mrsa11.pdf>
3. Schaible UE, Kaufmann SHE. Iron and microbial infection. Nat Rev Microbiol. 2004; 2:946–53. [PubMed: 15550940]
4. Ong ST, Ho JZS, Ho B, Ding JL. Iron-withholding strategy in innate immunity. Immunobiology. 2006; 211:295–314. [PubMed: 16697921]
5. Farrand AJ, Reniere ML, Ingmer H, Frees D, Skaar EP. Regulation of host hemoglobin binding by the Staphylococcus aureus Clp proteolytic system. J Bacteriol. 2013; 195:5041–50. [PubMed: 23995637]
6. Reniere ML, Torres VJ, Skaar EP. Intracellular metalloporphyrin metabolism in Staphylococcus aureus. Biometals. 2007; 20:333–45. [PubMed: 17387580]
7. Grigg JC, Ukpabi G, Gaudin CFM, Murphy MEP. Structural biology of heme binding in the Staphylococcus aureus Isd system. J Inorg Biochem. 2010; 104:341–8. [PubMed: 19853304]
8. Maresso AW, Schneewind O. Iron acquisition and transport in Staphylococcus aureus. Biometals. 2006; 19:193–203. [PubMed: 16718604]
9. Mazmanian SK, Ton-That H, Su K, Schneewind O. An iron-regulated sortase anchors a class of surface protein during Staphylococcus aureus pathogenesis. Proc Natl Acad Sci U S A. 2002; 99:2293–8. [PubMed: 11830639]
10. Mazmanian SK, Skaar EP, Gaspar AH, Humayun M, Gornicki P, Jelenska J, Joachmiak A, Missiakas DM, Schneewind O. Passage of heme-iron across the envelope of Staphylococcus aureus. Science. 2003; 299:906–9ma. [PubMed: 12574635]
11. Ton-That H, Marraffini LA, Schneewind O. Protein sorting to the cell wall envelope of Gram-positive bacteria. Biochim Biophys Acta. 2004; 1694:269–78. [PubMed: 15546671]
12. Dryla A, Gelbmann D, Von Gabain A, Nagy E. Identification of a novel iron regulated staphylococcal surface protein with haptoglobin-haemoglobin binding activity. Mol Microbiol. 2003; 49:37–53. [PubMed: 12823809]
13. Muryoi N, Tiedemann MT, Pluym M, Cheung J, Heinrichs DE, Stillman MJ. Demonstration of the iron-regulated surface determinant (Isd) heme transfer pathway in Staphylococcus aureus. J Biol Chem. 2008; 283:28125–36. [PubMed: 18676371]
14. Zhu H, Xie G, Liu M, Olson JS, Fabian M, Dooley DM, Lei B. Pathway for heme uptake from human methemoglobin by the iron-regulated surface determinants system of Staphylococcus aureus. J Biol Chem. 2008; 283:18450–60. [PubMed: 18467329]
15. Villareal, Va; Spirig, T.; Robson, SA.; Liu, M.; Lei, B.; Clubb, RT. Transient weak protein-protein complexes transfer heme across the cell wall of Staphylococcus aureus. J Am Chem Soc. 2011; 133:14176–9. [PubMed: 21834592]
16. Abe R, Caaveiro JMM, Kozuka-Hata H, Oyama M, Tsumoto K. Mapping the ultra-weak protein-protein interactions between heme transporters of Staphylococcus aureus. J Biol Chem. 2012; 287:16477–87. [PubMed: 22427659]
17. Reniere ML, Ukpabi GN, Harry SR, Stec DF, Krull R, Wright DW, Bachmann BO, Murphy ME, Skaar EP. The IsdG-family of haem oxygenases degrades haem to a novel chromophore. Mol Microbiol. 2010; 75:1529–38. [PubMed: 20180905]
18. Matsui T, Nambu S, Ono Y, Goulding CW, Tsumoto K, Ikeda-Saito M. Heme degradation by Staphylococcus aureus IsdG and IsdI liberates formaldehyde rather than carbon monoxide. Biochemistry. 2013; 52:3025–7. [PubMed: 23600533]
19. Andrade M, Ciccarelli F, Perez-Iratxeta C, Bork P. NEAT: a domain duplicated in genes near the components of a putative Fe3+ siderophore transporter from Gram-positive pathogenic bacteria. Genome Biol. 2002; 3:research0047.1–research0047.5. [PubMed: 12225586]
20. Pilpa RM, Robson SA, Villareal VA, Wong ML, Phillips M, Clubb RT. Functionally distinct NEAT (NEAr Transporter) domains within the Staphylococcus aureus IsdH/HarA protein extract heme from methemoglobin. J Biol Chem. 2009; 284:1166–76. [PubMed: 18984582]

21. Dryla A, Hoffmann B, Gelbmann D, Giefing C, Hanner M, Meinke A, Anderson AS, Koppensteiner W, Konrat R, von Gabain A, Nagy E. High-affinity binding of the staphylococcal HarA protein to haptoglobin and hemoglobin involves a domain with an antiparallel eight-stranded beta-barrel fold. J Bacteriol. 2007; 189:254–64. [PubMed: 17041047]
22. Krishna Kumar K, Jacques DA, Pishchany G, Caradoc-Davies T, Spirig T, Malmirchegini GR, Langley DB, Dickson CF, Mackay JP, Clubb RT, Skaar EP, Guss JM, Gell DA. Structural basis for hemoglobin capture by Staphylococcus aureus cell-surface protein, IsdH. J Biol Chem. 2011; 286:38439–47. [PubMed: 21917915]
23. Clarke SR, Wiltshire MD, Foster SJ. IsdA of Staphylococcus aureus is a broad spectrum, iron-regulated adhesin. Mol Microbiol. 2004; 51:1509–19. [PubMed: 14982642]
24. Nobles CL, Maresso AW. The theft of host heme by Gram-positive pathogenic bacteria. Metallomics. 2011; 3:788–96. [PubMed: 21725569]
25. Lei B. Benfang Lei's research on heme acquisition in Gram-positive pathogens and bacterial pathogenesis. World J Biol Chem. 2010; 1:286–90. [PubMed: 21537486]
26. Spirig T, Malmirchegini GR, Zhang J, Robson SA, Sjodt M, Liu M, Krishna Kumar K, Dickson CF, Gell DA, Lei B, Loo Ja, Clubb RT, Kumar KK. Staphylococcus aureus uses a novel multidomain receptor to break apart human hemoglobin and steal its heme. J Biol Chem. 2013; 288:1065–78. [PubMed: 23132864]
27. Gaudin CFM, Grigg JC, Arrieta AL, Murphy MEP. Unique heme-iron coordination by the hemoglobin receptor IsdB of Staphylococcus aureus. Biochemistry. 2011; 50:5443–52. [PubMed: 21574663]
28. Hargrove MS. Quaternary Structure Regulates Hemin Dissociation from Human Hemoglobin. J Biol Chem. 1997; 272:17385–17389. [PubMed: 9211878]
29. Dickson CF, Krishna Kumar K, Jacques DA, Malmirchegini GR, Spirig T, Mackay JP, Clubb RT, Guss JM, Gell DA. Structure of the Hemoglobin-IsdH Complex Reveals the Molecular Basis of Iron Capture by Staphylococcus aureus. J Biol Chem. 201410.1074/jbc.M113.545566
30. Hargrove MS, Singleton EW, Quillin ML, Ortiz LA, Phillips GN, Olson JS, Mathews AJ. His64(E7)-->Tyr apomyoglobin as a reagent for measuring rates of hemin dissociation. J Biol Chem. 1994; 269:4207–14. [PubMed: 8307983]
31. Spirig T, Clubb RT. Backbone (1)H, (13)C and (15)N resonance assignments of the 39 kDa staphylococcal hemoglobin receptor IsdH. Biomol NMR Assign. 201110.1007/s12104-011-9348-8
32. Clore GM, Iwahara J. Theory, practice, and applications of paramagnetic relaxation enhancement for the characterization of transient low-population states of biological macromolecules and their complexes. Chem Rev. 2009; 109:4108–39. [PubMed: 19522502]
33. Simon B, Madl T, Mackereth CD, Nilges M, Sattler M. An efficient protocol for NMR-spectroscopy-based structure determination of protein complexes in solution. Angew Chem Int Ed Engl. 2010; 49:1967–70. [PubMed: 20148424]
34. Volkov AN, Worrall JAR, Holtzmann E, Ubbink M. Solution structure and dynamics of the complex between cytochrome c and cytochrome c peroxidase determined by paramagnetic NMR. Proc Natl Acad Sci U S A. 2006; 103:18945–50. [PubMed: 17146057]
35. Page RC, Lee S, Moore JD, Opella SJ, Cross TA. Backbone structure of a small helical integral membrane protein: A unique structural characterization. Protein Sci. 2009; 18:134–46. [PubMed: 19177358]
36. Iwahara J, Schwieters CD, Clore GM. Ensemble approach for NMR structure refinement against (1)H paramagnetic relaxation enhancement data arising from a flexible paramagnetic group attached to a macromolecule. J Am Chem Soc. 2004; 126:5879–5896. [PubMed: 15125681]
37. Mackereth CD, Madl T, Bonnal S, Simon B, Zanier K, Gasch A, Rybin V, Valcárcel J, Sattler M. Multi-domain conformational selection underlies pre-mRNA splicing regulation by U2AF. Nature. 2011; 475:408–11. [PubMed: 21753750]
38. Bermejo GA, Strub MP, Ho C, Tjandra N. Determination of the solution-bound conformation of an amino acid binding protein by NMR paramagnetic relaxation enhancement: use of a single flexible paramagnetic probe with improved estimation of its sampling space. J Am Chem Soc. 2009; 131:9532–7. [PubMed: 19583434]

39. Dosset P, Hus JCC, Marion D, Blackledge M. A novel interactive tool for rigid-body modeling of multi-domain macromolecules using residual dipolar couplings. J Biomol NMR. 2001; 20:223–31. [PubMed: 11519746]
40. Schwieters CD, Clore GM. Using small angle solution scattering data in Xplor-NIH structure calculations. Prog Nucl Magn Reson Spectrosc. 2014; 80:1–11. [PubMed: 24924264]
41. Clore GM, Bewley CA. Using conjoined rigid body/torsion angle simulated annealing to determine the relative orientation of covalently linked protein domains from dipolar couplings. J Magn Reson. 2002; 154:329–35. [PubMed: 11846592]
42. Clore GM, Schwieters CD. Theoretical and computational advances in biomolecular NMR spectroscopy. Curr Opin Struct Biol. 2002; 12:146–153. [PubMed: 11959490]
43. Svergun D, Barberato C, Koch MH. CRYSOL - A program to evaluate X-ray solution scattering of biological macromolecules from atomic coordinates. J Appl Crystallogr. 1995; 28:768–773.
44. Schwieters CD, Clore GM. Reweighted atomic densities to represent ensembles of NMR structures. J Biomol NMR. 2002; 23:221–5. [PubMed: 12238594]
45. Fonner BA, Tripet BP, Eilers B, Stanisich J, Sullivan-Springhetti RK, Moore R, Liu M, Lei B, Copie V. Solution Structure and Molecular determinants of Hemoglobin Binding of the first NEAT Domain of IsdB in Staphylococcus aureus. Biochemistry. 2014; 53:3922–3933. [PubMed: 24871270]
46. Pilpa RM, Fadeev EA, Villareal VA, Wong ML, Phillips M, Clubb RT. Solution structure of the NEAT (NEAr Transporter) domain from IsdH/HarA: the human hemoglobin receptor in Staphylococcus aureus. J Mol Biol. 2006; 360:435–47. [PubMed: 16762363]
47. Watanabe M, Tanaka Y, Suenaga A, Kuroda M, Yao M, Watanabe N, Arisaka F, Ohta T, Tanaka I, Tsumoto K. Structural basis for multimeric heme complexation through a specific protein-heme interaction: the case of the third neat domain of IsdH from Staphylococcus aureus. J Biol Chem. 2008; 283:28649–59. [PubMed: 18667422]
48. Zhu H, Li D, Liu M, Copié V, Lei B. Non-Heme-Binding Domains and Segments of the Staphylococcus aureus IsdB Protein Critically Contribute to the Kinetics and Equilibrium of Heme Acquisition from Methemoglobin. PLoS One. 2014; 9:e100744. [PubMed: 24959723]
49. Bowden CF, Verstraete MM, Eltis LD, Murphy MEP. Hemoglobin binding and catalytic heme extraction by IsdB NEAT domains. Biochemistry. 201410.1021/bi500230f
50. Senturia R, Faller M, Yin S, Loo JA, Cascio D, Sawaya MR, Hwang D, Clubb RT, Guo F. Structure of the dimerization domain of DiGeorge critical region 8. Protein Sci. 2010; 19:1354–65. [PubMed: 20506313]
51. Reverter D, Lima CD. A basis for SUMO protease specificity provided by analysis of human Senp2 and a Senp2-SUMO complex. Structure. 2004; 12:1519–31. [PubMed: 15296745]
52. Ascoli F, Fanelli MR, Antonini E. Preparation and properties of apohemoglobin and reconstituted hemoglobins. Methods Enzymol. 1981; 76:72–87. [PubMed: 7329287]
53. Reisberg PI, Olson JS. Equilibrium binding of alkyl isocyanides to human hemoglobin. J Biol Chem. 1980; 255:4144–30. [PubMed: 7372671]
54. Antonini, E.; Brunori, M. Hemoglobin and Myoglobin in their Reactions with Ligands. Amsterdam, Netherlands North-holl: 1971. at <http://www.fisica.unipa.it/~emoglobina/epsilon.html>
55. Fabian M, Solomaha E, Olson JS, Maresso AW. Heme transfer to the bacterial cell envelope occurs via a secreted hemophore in the Gram-positive pathogen Bacillus anthracis. J Biol Chem. 2009; 284:32138–46. [PubMed: 19759022]
56. Nygaard TK, Blouin GC, Liu M, Fukumura M, Olson JS, Fabian M, Dooley DM, Lei B. The mechanism of direct heme transfer from the streptococcal cell surface protein Shp to HtsA of the HtsABC transporter. J Biol Chem. 2006; 281:20761–71. [PubMed: 16717094]
57. Delaglio F, Grzesiek S, Vuister GW, Zhu G, Pfeifer J, Bax A. NMRPipe: a multidimensional spectral processing system based on UNIX pipes. J Biomol NMR. 1995; 6:277–93. [PubMed: 8520220]
58. Keller R. The Computer Aided Resonance Assignment Tutorial. 2004
59. Goddard TD, Kneller DG. Sparky NMR Analysis Software. 2001

60. Cavanagh, J.; Fairbrother, WJ.; Palmer, AG., III; Skelton, NJ. Protein NMR Spectroscopy: Principles and Practice (Google eBook). Vol. 587. Academic Press; 1995.
61. Rückert M, Otting G. Alignment of Biological Macromolecules in Novel Nonionic Liquid Crystalline Media for NMR Experiments. J Am Chem Soc. 2000; 122:7793–7797.
62. Hansen MR, Mueller L, Pardi A. Tunable alignment of macromolecules by filamentous phage yields dipolar coupling interactions. Nat Struct Biol. 1998; 5:1065–74. [PubMed: 9846877]
63. Cordier F, Dingley AJ, Grzesiek S. A doublet-separated sensitivity-enhanced HSQC for the determination of scalar and dipolar one-bond J-couplings. J Biomol NMR. 1999; 13:175–80. [PubMed: 10070758]
64. Shen Y, Delaglio F, Cornilescu G, Bax A. TALOS+: a hybrid method for predicting protein backbone torsion angles from NMR chemical shifts. J Biomol NMR. 2009; 44:213–23. [PubMed: 19548092]
65. Konarev PV, Volkov VV, Sokolova AV, Koch MHJ, Svergun DI. PRIMUS: A Windows PC-based system for small-angle scattering data analysis. J Appl Crystallogr. 2003; 36:1277–1282.
66. Battiste JL, Wagner G. Utilization of site-directed spin labeling and high-resolution heteronuclear nuclear magnetic resonance for global fold determination of large proteins with limited nuclear overhauser effect data. Biochemistry. 2000; 39:5355–65. [PubMed: 10820006]
67. Shi L, Traaseth NJ, Verardi R, Gustavsson M, Gao J, Veglia G. Paramagnetic-based NMR restraints lift residual dipolar coupling degeneracy in multidomain detergent-solubilized membrane proteins. J Am Chem Soc. 2011; 133:2232–41. [PubMed: 21287984]
68. Chen H, Ji F, Olman V, Mobley CK, Liu Y, Zhou Y, Bushweller JH, Prestegard JH, Xu Y. Optimal mutation sites for PRE data collection and membrane protein structure prediction. Structure. 2011; 19:484–95. [PubMed: 21481772]
69. Reckel S, Gottstein D, Stehle J, Löhr F, Verhoefen MK, Takeda M, Silvers R, Kainosho M, Glaubitz C, Wachtveitl J, Bernhard F, Schwalbe H, Güntert P, Dötsch V. Solution NMR structure of proteorhodopsin. Angew Chem Int Ed Engl. 2011; 50:11942–6. [PubMed: 22034093]
70. Zhang W, Pochapsky SS, Pochapsky TC, Jain NU. Solution NMR structure of putidaredoxin-cytochrome P450cam complex via a combined residual dipolar coupling-spin labeling approach suggests a role for Trp106 of putidaredoxin in complex formation. J Mol Biol. 2008; 384:349–63. [PubMed: 18835276]
71. Göbl C, Madl T, Simon B, Sattler M. NMR approaches for structural analysis of multidomain proteins and complexes in solution. Prog Nucl Magn Reson Spectrosc. 2014; 80:26–63. [PubMed: 24924266]
72. Solomon I, Bloembergen N. Nuclear Magnetic Interactions in the HF Molecule. J Chem Phys. 1956; 25:261.
73. Gottstein D, Reckel S, Dötsch V, Güntert P. Requirements on paramagnetic relaxation enhancement data for membrane protein structure determination by NMR. Structure. 2012; 20:1019–27. [PubMed: 22560730]
74. Kroncke BM, Horanyi PS, Columbus L. Structural origins of nitroxide side chain dynamics on membrane protein α-helical sites. Biochemistry. 2010; 49:10045–60. [PubMed: 20964375]
75. Weiner EM, Robson S, Marohn M, Clubb RT. The Sortase A enzyme that attaches proteins to the cell wall of Bacillus anthracis contains an unusual active site architecture. J Biol Chem. 2010; 285:23433–43. [PubMed: 20489200]
76. Mandel AM, Akke M, Palmer AG III. Backbone Dynamics of Escherichia coli Ribonuclease HI: Correlations with Structure and Function in an Active Enzyme. J Mol Biol. 1995; 246:144–163. [PubMed: 7531772]
77. Brüschweiler R, Liao X, Wright PE. Long-range motional restrictions in a multidomain zinc-finger protein from anisotropic tumbling. Science. 1995; 268:886–9. [PubMed: 7754375]
78. Lee LK, Rance M, Chazin WJ, Palmer AG. Rotational diffusion anisotropy of proteins from simultaneous analysis of 15N and 13C alpha nuclear spin relaxation. J Biomol NMR. 1997; 9:287–98. [PubMed: 9204557]
79. Schwieters CD, Kuszewski JJ, Tjandra N, Clore GM. The Xplor-NIH NMR molecular structure determination package. J Magn Reson. 2003; 160:65–73. [PubMed: 12565051]

80. Emsley P, Cowtan K. Coot: model-building tools for molecular graphics. Acta Crystallogr D Biol Crystallogr. 2004; 60:2126–32. [PubMed: 15572765]

81. Clore GM, Schwieters CD. How much backbone motion in ubiquitin is required to account for dipolar coupling data measured in multiple alignment media as assessed by independent cross-validation? J Am Chem Soc. 2004; 126:2923–38. [PubMed: 14995210]

82. Schwieters CD, Clore GM. The VMD-XPLOR visualization package for NMR structure refinement. J Magn Reson. 2001; 149:239–44. [PubMed: 11318623]

83. Nilges M, Gronenborn AM, Brünger AT, Clore GM. Determination of three-dimensional structures of proteins by simulated annealing with interproton distance restraints. Application to crambin, potato carboxypeptidase inhibitor and barley serine proteinase inhibitor 2. Protein Eng. 1988; 2:27–38. [PubMed: 2855369]

84. Clore GM, Kuszewski J. Chi(1) rotamer populations and angles of mobile surface side chains are accurately predicted by a torsion angle database potential of mean force. J Am Chem Soc. 2002; 124:2866–7. [PubMed: 11902865]

85. Schwieters CD, Suh JY, Grishaev A, Ghirlando R, Takayama Y, Clore GM. Solution structure of the 128 kDa enzyme I dimer from Escherichia coli and its 146 kDa complex with HPr using residual dipolar couplings and small- and wide-angle X-ray scattering. J Am Chem Soc. 2010; 132:13026–45. [PubMed: 20731394]

86. Schwieters CD, Clore GM. Internal coordinates for molecular dynamics and minimization in structure determination and refinement. J Magn Reson. 2001; 152:288–302. [PubMed: 11567582]

87. Deshmukh L, Schwieters CD, Grishaev A, Ghirlando R, Baber JL, Clore GM. Structure and dynamics of full-length HIV-1 capsid protein in solution. J Am Chem Soc. 2013; 135:16133–47. [PubMed: 24066695]

88. Koradi R, Billeter M, Wüthrich K. MOLMOL: a program for display and analysis of macromolecular structures. J Mol Graph. 1996; 14:51–5. 29–32. [PubMed: 8744573]

89. DeLano, WL. The PyMOL Molecular Graphics System, Version 1.5.0.04. Schrödinger LLC; 2002. http://www.pymol.org

90. Laskowski RA, Rullmannn JA, MacArthur MW, Kaptein R, Thornton JM. AQUA and PROCHECK-NMR: programs for checking the quality of protein structures solved by NMR. J Biomol NMR. 1996; 8:477–86. [PubMed: 9008363]

91. Chen VB, Arendall WB, Headd JJ, Keedy DA, Immormino RM, Kapral GJ, Murray LW, Richardson JS, Richardson DC. MolProbity: all-atom structure validation for macromolecular crystallography. Acta Crystallogr D Biol Crystallogr. 2010; 66:12–21. [PubMed: 20057044]

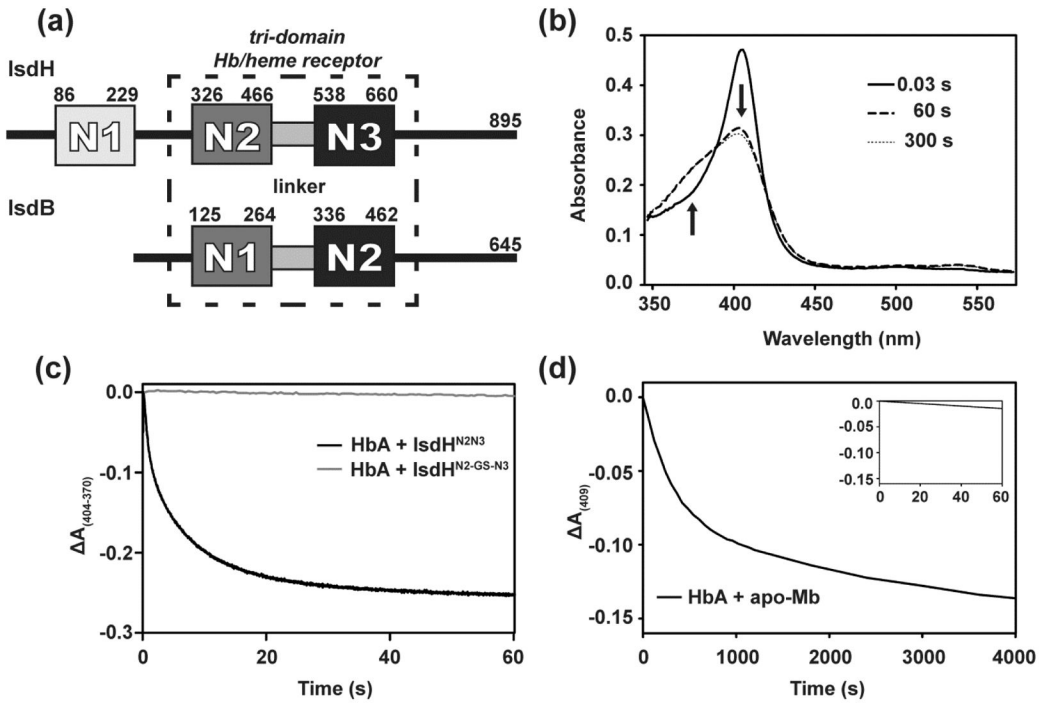

Figure 1. *S. aureus* uses conserved tri-domain receptors to rapidly capture hemin from Hb

(*a*) Schematic of the conserved NEAT domains of *S. aureus* Hb receptors, IsdH and IsdB. NEAT domains that bind Hb and hemin (oxidized form of heme) are shown in gray and black, respectively. Residue numbers of the functionally homologous NEAT domains as well as the linker connecting them are indicated. (*b*) Rapid spectral changes in UV-Vis spectrum of the reaction of 1.5 μM metHb and 6.5 μM apo-IsdH^{N2N3}. Arrows indicate the increase and decrease over time for the absorbances at 370 and 404 nm, respectively. (c) Time course of the $\Delta A_{404\text{-}370}$ change after mixing 1.5 μM metHb and 6.5 μM apo-IsdH^{N2N3} (black line). The data was fit to a double-exponential equation and yielded hemin transfer rates of 0.85 ± 0.11 and 0.099 ± 0.14 s^{-1}. Similar hemin transfer data is shown for the reaction containing 1.5 μM metHb and 6.5 μM apo-IsdH$^{N2\text{-}GS\text{-}N3}$, a IsdH^{N2N3} mutant in which the linker is replaced with a glycine-serine nonapeptide (grey line). (d) Time course of the ΔA_{409} change after mixing 2.5 μM HbA and 40 μM H64Y/V68F apo-Mb. The first 60 seconds of the reaction is shown in the inset for comparison.

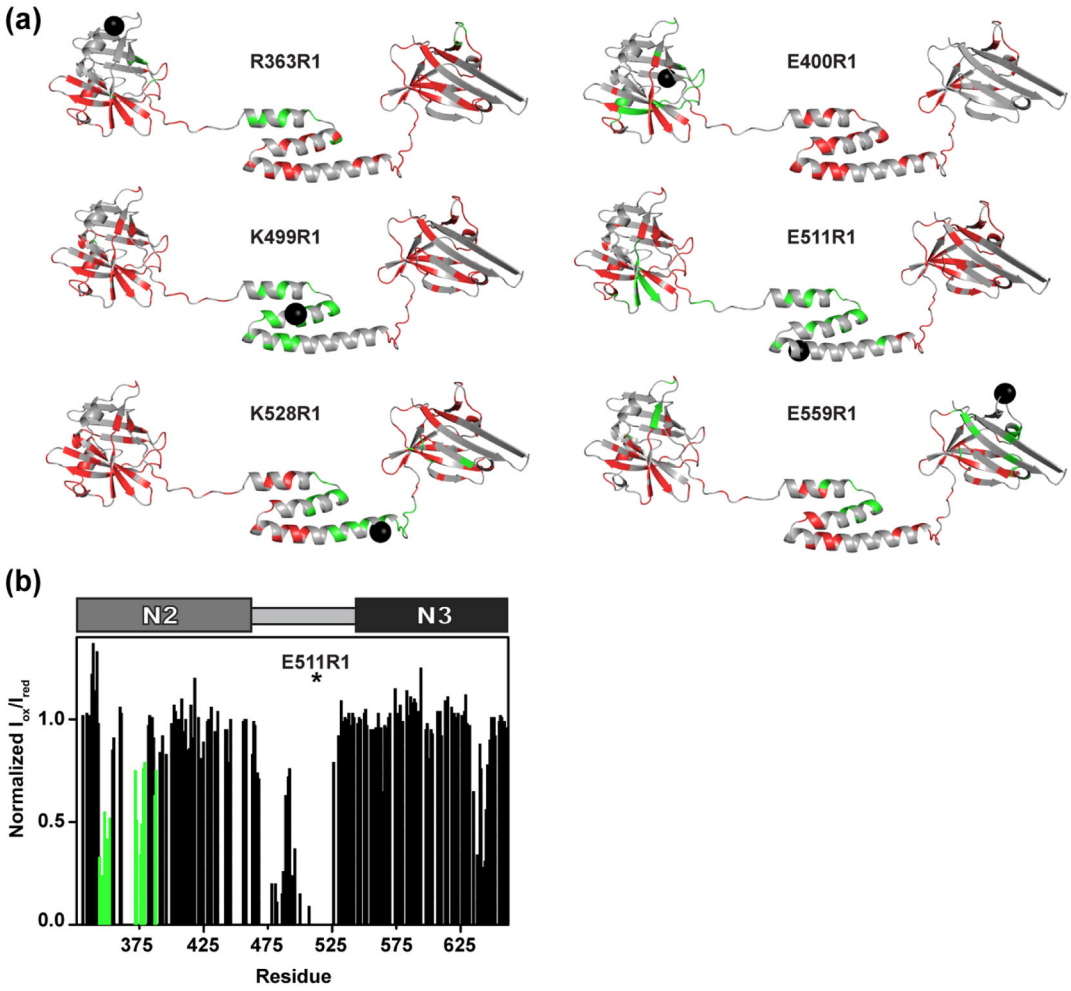

Figure 2. NMR spectra of IsdH^{N2N3}

(*a*) A representative ^{15}N-HSQC of IsdH^{N2N3}. Boxed regions indicate the representative sections of each PRE probe's spectra shown in (*b*) (E511R1 and R363R1 probes). (*b*) Magnified regions depicting selective distance dependent line-broadening for the E511R1 (bottom) and R363R1 (top) probes. For each probe selected diamagnetic and paramagnetic spectra are shown in the left and right panels, respectively. (*c*) Representative NMR spectra of inter-domain methyl-edited NOEs in IsdH^{N2N3}. Panels show regions within the ^{13}C-edited NOESY. Methyl-amide NOEs were cross validated in the ^{15}N-edited NOESY spectra. The N2-linker interface is shown in the right panel and the linker-N3 interface in shown in the left panel. Inter-domain NOEs are labeled and any intra-domain NOEs or apodization effects were left unlabeled.

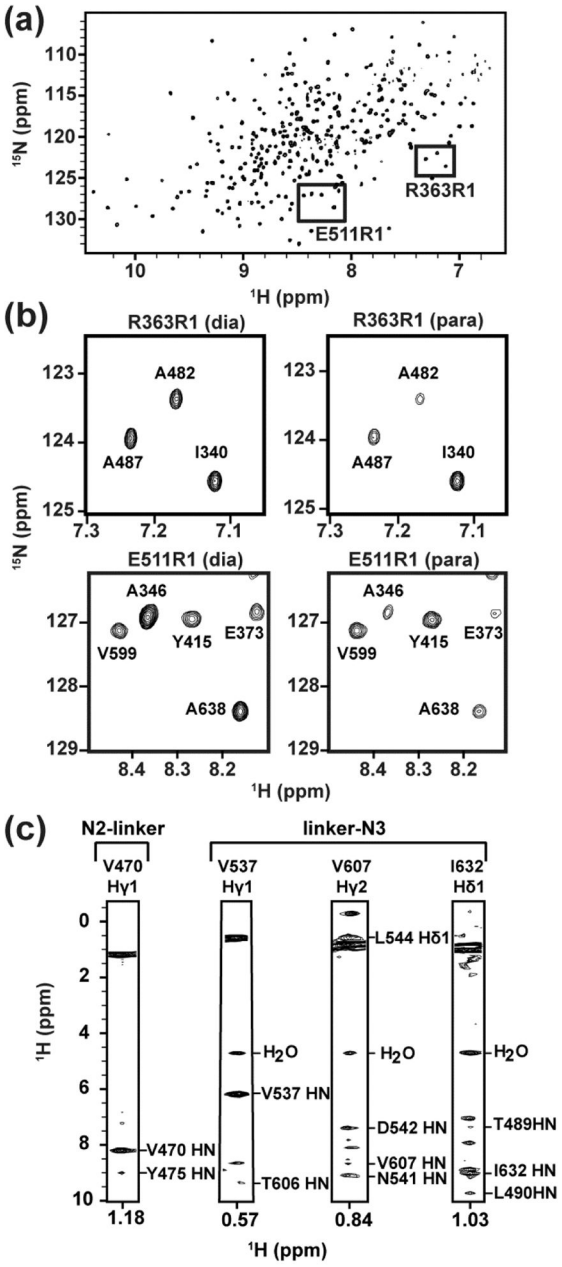

Figure 3. IsdH^{N2N3} PRE profile for each probe

(*a*) The distance-dependent line-broadening effect observed by each spin-label mutant is mapped to the extended starting structure of IsdH^{N2N3}. Attractive PRE effects (I_{ox}/I_{red} < 0.80) are shown in green and repulsive PRE effects ($I_{ox}/I_{red} \geq 0.80$) are shown in red. The alpha carbon of each residue where the probe is located is depicted as a black sphere. Residues to which no PRE information is available are shown in grey. Mapping data for the following probes is shown: R363R1, E400R1, K499R1, E511R1 K528R1, and E559R1. (*b*) representative PRE profile of the E511R1 probe data. Normalized PRE intensity ratios (I_{ox}/I_{red}) are shown as a function of residue number. The domain boundaries are shown in schematic above. The asterisk denotes the location of the probe. Green bars indicate the

effect seen in the N2 domain that is not reflected in the crystal structure. Errors in the ratio measurements are approximately 10–15% based on signal to noise of the NMR spectra, and thus can lead to values in excess of 1. Errors in the intensity ratio can also occur as a result of manipulating the sample (adding ascorbic acid to oxidize the probe) and instrument instability. These errors are partially accounted for by adding ± 5.0 Å to the distance restraints that are obtained from the ratio data.

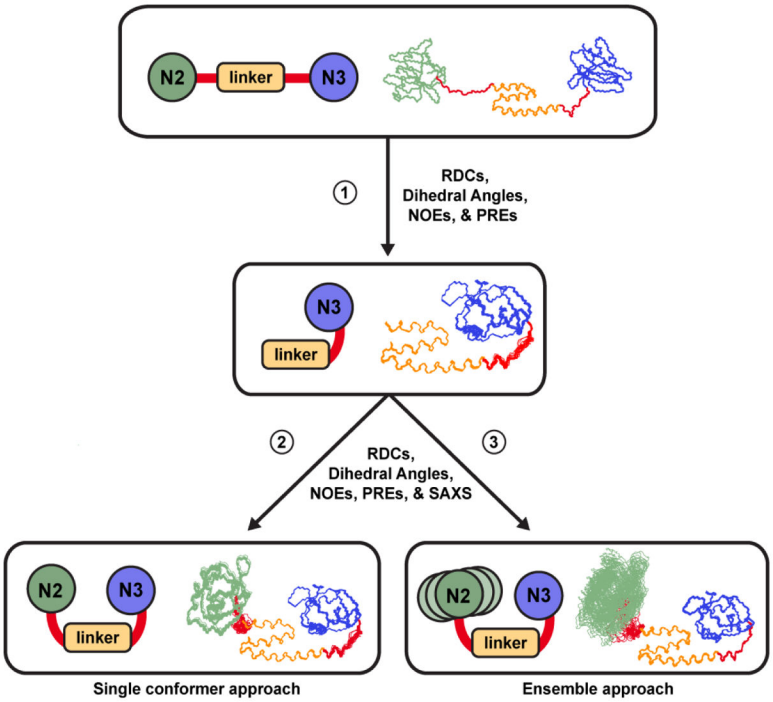

Figure 4. Schematic of the calculation strategy used to model the structure of IsdH^{N2N3}

In step (1), the structure of the linker-N3 inter-domain interface was determined using the appropriate NMR experimental restraints. In step (2), the coordinates from step (1) were used as input and only the structure of the N2-linker interface was refined against the NMR and SAXS data. The structure of the linker-N3 interface determined in step (1) is compatible with the experimental data, whereas the structure of the intact protein produced from step (2) exhibits slight, but systematic violations with the PRE distance data that originate from residues or probes located in the N2 domain (eight restraints have violations ranging from 0.5 to 2.7 Å). To account for this discrepancy, in step (3) ensemble calculations were performed in which the N2-linker interface calculations were using four molecular structures to represent the receptor. Color code: the N2, linker and N3 domains are colored green, yellow and blue, respectively, and the coordinates of residues that connect the domains are colored red (I462-Y475 connecting the N2 and linker domains and V531-Q543 connecting the linker and N3 domains).

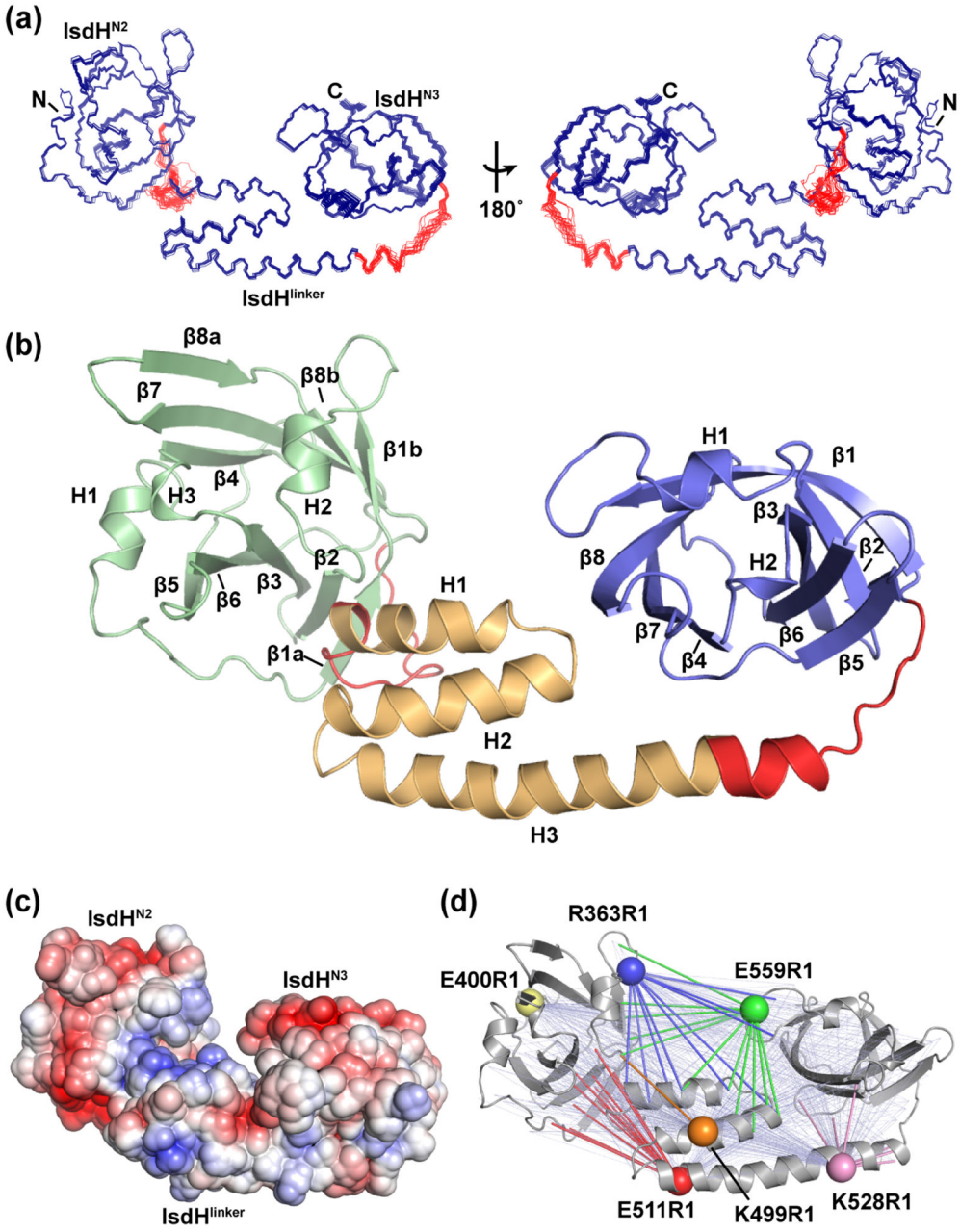

Figure 5. NMR structure model of a *S. aureus* tri-domain hemoglobin receptor, IsdH^{N2N3}

(*a*) The ensemble of the top 20 lowest energy structures for IsdH^{N2N3} calculated using the two step procedure outlined in Fig. 4 (steps 1 and 2). The connector regions between each domain that were allowed to move during the conjoined rigid-body/torsion angle dynamics are colored in red. Two views are shown related by a 180° rotation. (*b*) Ribbon diagram of the lowest energy structure of IsdH^{N2N3}. The N2, linker, and N3 domains are colored in green, yellow, and blue, respectively. The residues connecting the domains are colored in red. Secondary structure elements are labeled for each subdomain. (*c*) Electrostatic surface of IsdH^{N2N3} showing positively and negatively charged residues colored in blue and red,

respectively. (*d*) Graphical summary of the PRE-derived distance restraint data used to determine the structure showing its compatibility with the NMR structure. Data from probes providing attractive distance restraints are indicated by bold lines originating from spheres that correspond to the backbone position of each probe: R363R1 (dark blue), E400R1 (yellow), E511R1 (red), K528R1 (pink) and E559R1 (green). Repulsive restraints are shown as light blue lines. Only inter-domain attractive and repulsive restraints are shown. The structures shown in panels (*b* to *d*) are presented in the same orientation and were generated using the program PyMOL[89].

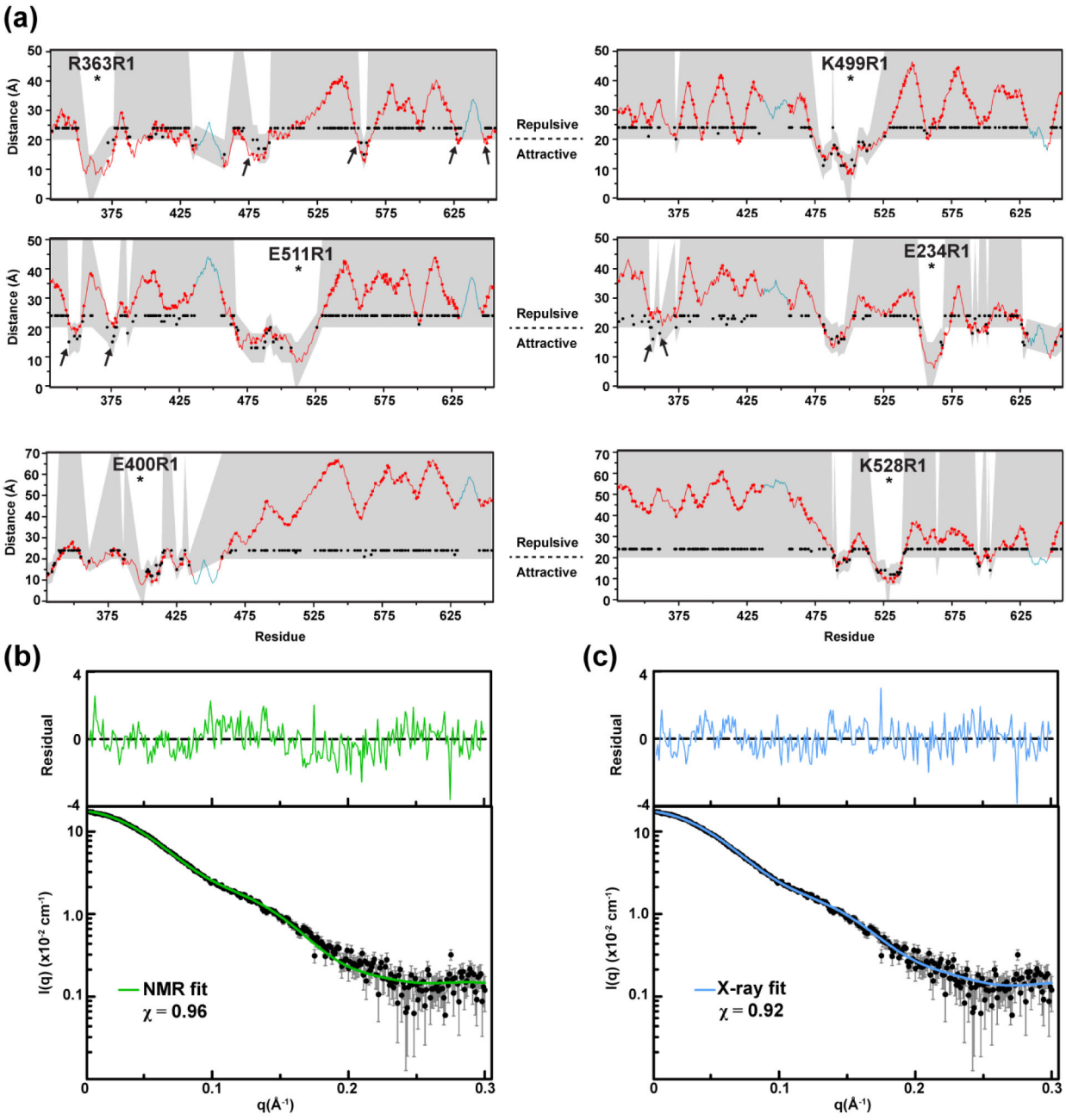

Figure 6. Compatibility of the structure of IsdH^{N2N3} with the PRE and SAXS data

(*a*) For each probe the panels as a function of residue number a graph of the distance between the backbone amide protons to each probe in the top 20 lowest energy NMR structures (red dots). Standard deviations are represented by error bars and in some cases are too small to be seen. The shaded regions indicate the range of the PRE-derived distance restraints used in the calculation between the probe and amide proton, while the PRE-derived distance is indicated by a black dot. Repulsive restraints span a wide range of distances (upper half of each figure); while attractive restraints are assigned narrower ranges of ± 5.0 Å (bottom half each panel). Distances in the structure indicated by a blue line

correspond to residues in the ligand binding pockets and were not used in the NMR calculations. Each panel shows a violation analysis for one probe whose name is indicated on the upper half of the figure. Arrows indicate eight PRE-derived distance restraints that were systematically violated in ensemble by 0.5 to 2.7 Å (also partially shown in Fig. 7A). (*b*) Fit of the experimental solution scattering of $IsdH^{N2N3}$ to the theoretical scattering curve (colored in green) of the NMR structure ($\chi = 0.96$). The residual of the fit is shown at the top of the figure. The data was analyzed using the programs CalcSAXS[40] and CRYSOL[43]. (*c*) As in panel (*b*), but the coordinates of the crystal structure of the receptor in the $IsdH^{N2N3}$:Hb complex (PDB code: 4IJ2) were used to generate the theoretical scattering curve ($\chi = 0.92$, colored green).

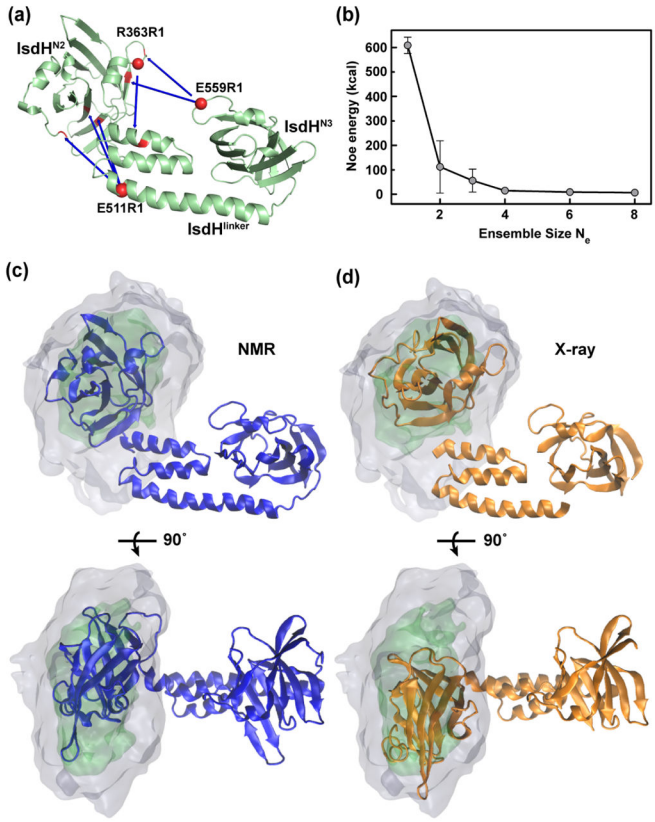

Figure 7. Estimation of the N2 domain motions in the Hb-free receptor

(a) Six of the 8 consistently violated PRE-derived distance restraints mapped onto the lowest energy structure calculated from the two-step procedure. The blue arrows point toward the location of each violated restraint (backbone atoms colored red) that originate from the E511R1, R363R1 and E559R1 probes (shown in red spheres). (b) The top 15 calculated NOE energies as a function of ensemble size with the standard deviation shown in bars, where ensemble sizes greater than 4 results in error bars are too small to be seen. (c and d) The estimated domain motions of the N2 domain are shown as a reweighted atomic probability density map plotted at 50% (green) and 10% (grey) of maximum. Two views are shown related by a 90° rotation. A cartoon representation of the single conformer Hb-free NMR model is shown in blue in panel (c), whereas a single receptor molecule from the crystal structure of the $IsdH^{N2N3}$:Hb tetrameric complex (PDB code: 4IJ2, chain G) is shown in orange in panel (d).

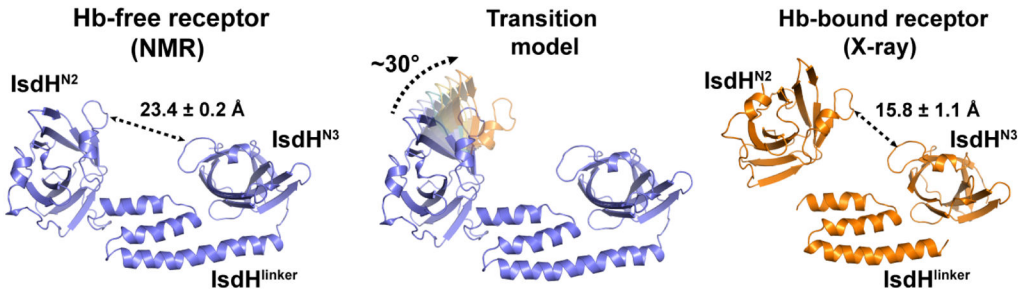

Figure 8. Structural differences between the Hb-free and -bound forms of IsdH^{N2N3}

The NMR apo-model of IsdH^{N2N3} is shown in blue (left) and a single receptor molecule from the crystal structure of the IsdH^{N2N3}:Hb tetrameric complex (PDB code: 4IJ2, chain G) is shown in orange (right). The distances shown are from the alpha carbon atoms of residues E362 and E559. The transition from the free form of the receptor into a more compact bound form is modeled in the figure by showing hypothetical structural intermediates of the Hb binding pocket in N2 (middle). Structural intermediates were calculated using the Rigimol plugin for PyMOL[89].

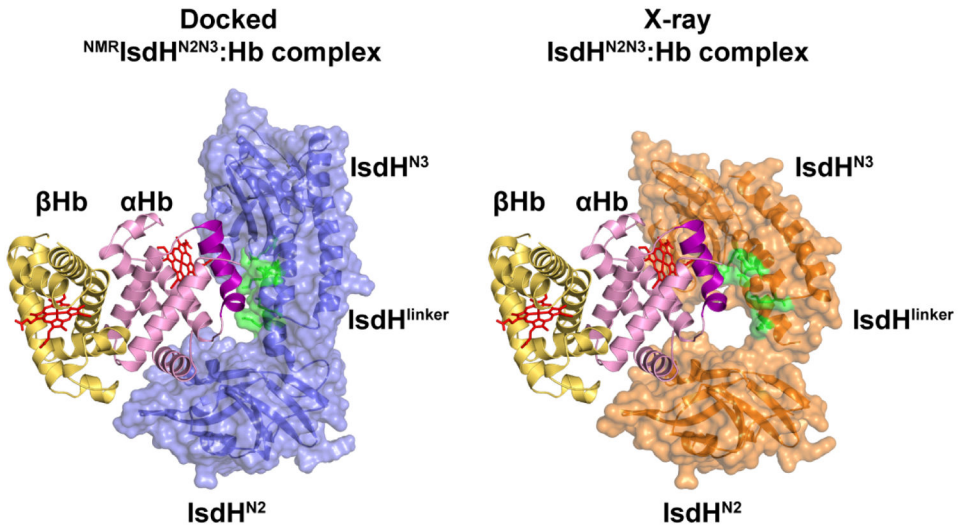

Figure 9. Model of hemin extraction by IsdH^{N2N3}

The panel on the left shows a hypothetical structure of the complex between the NMR model of IsdH^{N2N3} (blue) and dimeric Hb (αHb in pink with the F-helix colored in purple and βHb in yellow). The model was generated by superimposing the coordinates of the N2 domain in the NMR model and crystal structure of the IsdH^{N2N3}:Hb complex (PDB code: 4IJ2, chain G). The panel on the right shows the structure of the IsdH^{N2N3}:Hb complex for comparison (only one receptor is shown). The protein backbones of the receptors are shown in schematic and surface representation. The globin chains of Hb are shown in schematic and the hemin groups are colored red and shown in stick representation. Residues within the linker domain of IsdH^{N2N3} that are atomically overlapping with αHb are also shown in stick representation and colored green.

Table 1

Predicted and experimental correlation times for the domains within IsdH^{N2N3}

τ_c (ns)	N2	N3	N2-linker-N3 (IsdH^{N2N3})
Experimental	13.9 ± 0.1	15.5 ± 0.1	16.3 ± 0.1
Predicted[†]	8.4[a] (7.1[b])	7.3[a] (6.0[b])	17.9[a](16.0[b])

[†]Predicted correlation times calculated from equations based on a spherical protein using either

[a]molecular weight[88] or

[b]temperature and number of amino acid residues[89].

Table 2

Structural statistics for linker and N3 domain-domain interface in IsdH^{N2N3}

PRE distance restraints	**R363R1**	**E400R1**	**K499R1**	**E511R1**	**K528R1**	**E559R1**
# of restraints	0	0	66	67	62	22
# of violations > 0.5 Å[a]	0	0	0	0	0	0
PRE *Q*-factor[b]	n/a	n/a	0.09	0.07	0.15	0.11
NOE distance restraints	**NOEs**					
# of restraints[c]	13/7					
# of violations > 0.5 Å[a]	0					
Orientational restraints						
Total ^{1}H-^{15}N residual dipolar couplings	44					
PEG C12E5/hexanol	20					
pf1 phages	22					
Dihedral Angles (Φ and Ψ)	24					
RDC *R-factor*						
PEG C12E5/hexanol	3.60 ± 0.03					
pf1 phages	11.7 ± 0.05					
PROCHECK-NMR results (%)[d]						
most favorable region	90.0 ± 0.6					
additionally allowed region	10.0 ± 0.6					
generously allowed region	0.0 ± 0.0					
disallowed region	0.0 ± 0.0					
Coordinate Precision (Å)[e]						
Protein back bone (N476-I655)	0.37 ± 0.11					
Protein heavy atoms (N476-I655)	0.68 ± 0.11					

[a] Average number of distance restraints violated in the 20 lowest energy structures.

[b] Quality factor of experimental I_{ox}/I_{red} vs. back-calculated I_{ox}/I_{red} of the ensemble. Only inter-domain restraints were included.

[c] Total number of restraints, with the number of inter-domain restraints indicated after the slash.

[d] PROCHECK-NMR^{90} includes residues (N476-I655).

[e] The coordinate precision is defined as the average atomic root mean square deviation (RMSD) of the 20 individual simulated annealing structures and their mean coordinates. Backbone atoms are N, C^{α}, C′, and O. During the calculation the backbone coordinates of the linker (N476-A530) and N3 (L544-I655) were treated as rigid bodies.

Table 3

Structural statistics for intact $IsdH^{N2N3}$

PRE distance restraints	**R363R1**	**E400R1**	**K499R1**	**E511R1**	**K528R1**	**E559R1**
# of restraints[a]	87	83	133(67)	130(63)	130(68)	66(44)
# of violations > 0.5 Å[b]	4.2	0	0.8	2.9	0	2
Maximum violation (Å)	2.4	n/a	0.94	1.8	n/a	2.7
PRE *Q*-factor[c]	0.24	0.07	0.10	0.12	0.13	0.14
NOE distance restraints	**NOEs**					
# of restraints[d]	19/8					
N2-LN3[d]	6/1					
L-N3[d]	13/7					
# of violations > 0.5 Å[b]	0					
Orientational restraints[a]						
Total ^{1}H-^{15}N residual dipolar couplings	108(64)					
PEG C12E5/hexanol	40(20)					
pf1 phages	68(46)					
Dihedral Angles (Φ and Ψ)	50(26)					
RDC*R-factor*						
PEG C12E5/hexanol	9.9 ± 0.4					
pf1 phages	16.9 ± 0.8					
SAXS						
CRYSOL[e] χ	0.96					
PROCHECK-NMR results (%)[e]						
most favorable region	87.9 ± 0.6					
additionally allowed region	12.1 ± 0.6					
generously allowed region	0.0 ± 0.0					
disallowed region	0.0 ± 0.0					
Molprobity (%) [e]						
Ramachandran outliers	0.0 ± 0.0					

Ramachandran favored	91.13
Bad backbone (%)	0.13
Coordinate Precision (Å)[g]	
Protein back bone (A326-I655)	0.40 ± 0.11
Protein heavy atoms (A326-I655)	0.73 ± 0.09

[a] Total number of restraints, with the number of restraints to the N2 domain indicated in parentheses.

[b] Average number of distance restraints violated in the 20 lowest energy structures.

[c] Quality factor of experimental I_{ox}/I_{red} vs. back-calculated I_{ox}/I_{red} of the ensemble. Only inter-domain restraints were included.

[d] Total number of restraints, with the number of inter-domain restraints indicated after the slash.

[e] Fit to the experimental scattering curve for the lowest energy structure using CRYSOL[43]. The goodness of fit to the experimental scattering curve for each of the 20 individual simulated annealing structures was also measured using the CalcSAXS helper program in the XPLOR-NIH (v. 2.37) software package[40,78] and yielded values of $\chi^2 = 0.81 \pm 0.02$.

[e] PROCHECK-NMR[90] and Molprobity[91] results includes residues (A326-I655) and are of acceptable quality for an NMR structure.

[g] The coordinate precision is defined as the average atomic root mean square deviation (RMSD) of the 20 individual simulated annealing structures and their mean coordinates. Backbone atoms are N, C^{α}, C′, and O. During the calculation the backbone coordinates of the N2 domain (A326-P461) and residues spanning the linker and N3 domains (N476-I655) were treated as rigid bodies. The coordinates spanning the linker and N3 domains were derived from the calculation described in Table 2.